Impaired envelope integrity in the absence of SanA is linked to increased Lipid II availability and an imbalance of FtsI and FtsW activities

Joseph F. Carr[a], Carolina Basurto De Santiago[a,‡], Shivani A. Bhut[a,‡], Daniel J. Warzecha[a,‡] Robert Wei[a], Carmen M. Herrera[b], M. Stephen Trent[b,c], Beiyan Nan[a], Angela M. Mitchell[a,#]

[a] Department of Biology, Texas A&M University, College Station, Texas, USA

[b] Department of Infectious Diseases, College of Veterinary Medicine, University of Georgia, Athens, Georgia, USA

[c] Department of Microbiology, College of Art and Sciences; University of Georgia, Athens, Georgia, USA

Running Title: Envelope permeability from altered septum synthesis

Address correspondence to Angela M. Mitchell, amitchell@bio.tamu.edu

[‡] Authors contributed equally to this work. Order was determined alphabetically.

Abstract: 240 words

Main Text: 6659 words

ABSTRACT

In gram-negative bacteria, the outer membrane (OM) acts in conjunction with the peptidoglycan (PG) cell wall as a barrier against physical, osmotic, and toxic environmental stresses including antibiotics. SanA, an inner membrane protein in *Escherichia coli* K-12, is required for vancomycin resistance at high temperatures (>42 °C) and we have previously demonstrated that SanA impacts sodium dodecyl sulfate (SDS) resistance during stationary phase reached from carbon limitation. However, its function remains unknown. Here, we show that Δ*sanA* has a synthetic genetic interaction with Δ*wecA*, a mutation increasing the availability of the isoprenoid carrier for PG biosynthesis. Specifically, the Δ*sanA* Δ*wecA* strain demonstrated heightened SDS EDTA sensitivity, Rcs stress response activation, and increased cell length. Further investigation tied the SDS EDTA sensitivity to increased Lipid II available for PG synthesis. Spontaneous suppressor mutants of this phenotype harbored point mutations in *prc* which encodes tail specific protease or *ftsI* which encodes the cell division DD-transpeptidase, a target of Prc. Given Prc's role in FtsI maturation, we focused on the *ftsI* mutations and determined these mutations caused a partial loss of function in FtsI, with at least one of these mutations also increasing FtsW activity. Moreover, we found that other mutations which reduce septal PG synthesis, but not divisome assembly, also suppressed the SDS EDTA sensitivity. Together, these findings demonstrates that, in the absence of SanA, increased Lipid II availability perturbs the balance between FtsI and FtsW function leading to increased OM permeability.

45 **IMPORTANCE**

46 The gram-negative cell envelope is a barrier that protects the cell from environmental stress
47 and the synthesis of each layer of this envelope needs to be carefully coordinated
48 throughout growth and division. Here, we investigated the function of a protein in *Escherichia*
49 *coli* K-12, SanA, that affects envelope permeability in conditions of cellular stress, including
50 nutrient limitation and growth at high temperature. We found SanA is important for envelope
51 permeability when higher levels of the precursor for peptidoglycan cell wall synthesis are
52 expected, and that the permeability is linked to an imbalance in septal peptidoglycan
53 synthesis during cell division. Overall, our results show that excess availability of substrate
54 for septal peptidoglycan synthesis can impede proper septum synthesis leading to envelope
55 permeability and that SanA modulates the substrate availability to maintain the envelope
56 permeability barrier.

57

58 **INTRODUCTION**

59 Gram-negative bacteria have a multi-layered envelope consisting of the inner or cytoplasmic
60 membrane (IM), the aqueous periplasm containing the peptidoglycan (PG) cell wall, and the
61 outer membrane (OM) (1). While the IM is a phospholipid bilayer, the lipid portion of the OM
62 is composed of phospholipids in the inner leaflet and lipopolysaccharide (LPS) in the outer
63 leaflet. The cell envelope is tightly interconnected. For instance, the OM and the cell wall are
64 physically connected by an OM lipoprotein (Lpp) and/or outer membrane proteins (OMPs)
65 that bind to PG (e.g., OmpA) (2, 3). When the envelope is properly composed, it prevents the
66 entry of toxic molecules, resists osmotic and physical stress, and facilitates cell growth, all
67 while allowing nutrients to enter the cell and metabolic waste to be expelled (1, 4-8). The
68 envelope permeability barrier prevents the entry of molecules that are either large or
69 hydrophobic, making gram-negative bacteria intrinsically resistant to many clinically used
70 antibiotics and greatly complicating the discovery of new antimicrobials (4). Yet, the
71 pathways responsible for envelope biogenesis and the regulatory interactions between the
72 biogenesis pathways are promising targets for development of new antimicrobials (9-17).

73 There are separate pathways for the synthesis of each component of the layers of the
74 envelope (1, 18-21); however, recent work has demonstrated there are complex regulatory
75 interactions between the envelope biogenesis pathways that allow the growth of the layers
76 to be coordinated (22). For instance, in *Escherichia coli*, halting fatty acid synthesis, and so
77 the synthesis of phospholipids and LPS, causes PG synthesis to cease (23). In fact, synthesis
78 of phospholipids in excess of those needed for the IM and inner leaflet of the OM can trigger
79 PG expansion through phospholipids in the outer leaflet of the OM acting as a signal to
80 activate MepS, an endopeptidase that breaks PG crosslinks to allow new PG insertion (24).
81 Interestingly, cell growth can be separated from new PG synthesis and endopeptidase
82 activity and cell growth can continue in the absence of PG synthesis until the point of cell
83 lysis (25). The physical strength of the OM also plays a role in orienting PG synthesis and LPS
84 mutations strengthening the OM can restore rod shape in mutants deficient in activation of
85 the elongasome, which is responsible for PG synthesis during cell growth (26). YhcB (a.k.a.

86 ZapG, LapD) has been suggested to interact with both the elongasome and with the complex
87 responsible for regulating LPS synthesis and has been suggested to play a role in balancing
88 the production of LPS, PG, and phospholipids (27-29). In *Pseudomonas aeruginosa*, the
89 interactions between PG and LPS biosynthesis are more direct with physical interaction
90 between MurA, which catalyzes the first committed step in PG biosynthesis, and LpxC,
91 which catalyzes the first committed step in LPS biosynthesis, causing stimulation of LpxC
92 activity (30). Interactions in biosynthesis can also occur based on the use of shared
93 synthesis substrates. For instance, most extracytoplasmic glycans are synthesized on an
94 isoprenoid carrier, undecaprenyl-phosphate (Und-P), and mutations that affect biosynthesis
95 of one glycan can disrupt synthesis of the others due to sequestration of Und-P. For instance,
96 mutations in later steps of enterobacterial common antigen (ECA) synthesis cause cell
97 shape defects and envelope stress response activation, presumably through the inhibition
98 of PG synthesis (31-36). Investigation of the level of Und-P has shown that mutation of the
99 gene for the first step in ECA synthesis (*wecA*) causes approximately a 2-fold increase in free
100 Und-P and that levels decrease from that point in later pathway mutations (37).

101 The need for coordination in synthesis of the layers of the cell envelope becomes more acute
102 during conditions that perturb synthesis of envelope components such as nutritional stress
103 or cell division. PG synthesis during cell division is carried out by a highly regulated complex
104 known as the divisome (38, 39). The divisome is assembled on the FtsZ ring which consists
105 of FtsZ, FtsA, and ZipA in *E. coli*. FtsK is then recruited, followed by FtsQ, FtsL, and FtsB.
106 Once this complex is complete, FtsW, FtsI, and FtsN then join the complex. FtsW and FtsI
107 (PBP3) are responsible for synthesis of the septal PG with FtsW acting as the
108 transglycosylase linking the glycan backbone of PG and FtsI acting as the DD-transpeptidase
109 to link the peptide stems of the PG. FtsA plays a key role in recruiting the downstream
110 components of the complex, while recruitment of FtsN acts as a signal to begin cell division.

111 As septal PG synthesis occurs, the OM invaginates with the PG allowing for coordinated
112 separation of the cell envelope (39). This coordination is accomplished through a protein,
113 CpoB, that interacts with LpoB and PBP1B at the septum and with the Tol-Pal complex, which

114 has IM and OM components and contacts PG (40-42). Beyond its importance for OM
115 invagination, Tol-Pal, as well as two OM lipoproteins (NlpD and YraP), are involved in the
116 activation of amidases that split the septal PG during cell division, ensuring the coordination
117 of OM invagination with cell division (43, 44). Interestingly, mutations inactivating NlpD led
118 to increased sensitivity to the detergent SDS in combination with EDTA, which disrupts
119 interactions between LPS molecules, suggesting that the OM permeability barrier is
120 disrupted by this mutation (43). To complete the invagination of the OM, an increase in OM
121 synthesis is required. The folding of OMPs into the OM by the β-barrel assembly machine
122 (BAM) is activated by immature PG allowing the insertion of new OMPs into the OM to be
123 increased at the cell septum facilitating this increased synthesis (45). In combination with
124 the regulatory mechanisms mentioned above, this is likely to allow balanced synthesis of
125 OM during the cell division process.

126 We previously investigated changes in OM permeability during stationary phase initiated by
127 carbon limitation (46). We found that resistance to SDS during carbon limitation did not rely
128 on efflux pumps as it did in exponentially growing cells. Instead, a change in OM permeability
129 dependent on RpoS, the master regulator of stationary phase, occurred and required the
130 presence of three genes, *sanA*, *dacA* (PBP5), and *yhdP* (46). YhdP is now a proposed inter-
131 membrane phospholipid transporter (47-50), the loss of which causes increased OM
132 permeability in the presence of ECA (51). PBP5 is a carboxypeptidase that cleaves D-alanine
133 from the PG pentapeptide, regulating the amount of substrate available for transpeptidases
134 (52). Later work has shown that loss of PBP5 can prevent the maturation of PG that results in
135 mid-cell insertion of new OMP proteins (45). Together, these findings suggest that envelope
136 coordination is important for the stationary phase membrane permeability effects of the
137 mutations we identified. With this in mind, we have turned our attention to *sanA*, a gene of
138 unknown function.

139 SanA is a bitopic inner membrane protein that has one N-terminal transmembrane helix and
140 a periplasmic domain consisting of a DUF218 domain (53, 54). In *E. coli* K-12, *sanA* was first
141 identified as a multicopy suppressor of vancomycin sensitivity in a strain with a gene

142 deletion that included *sanA* (55). It was also found to be involved in vancomycin resistance
143 at high temperature (i.e., 43 °C) (55). In *Salmonella enterica* serovar Typhimurium, SfiX
144 (homologous to SanA) is necessary for filamentation of a mutant overexpressing *hisFH* (His^C)
145 and also affects vancomycin resistance at high temperature (56). More recent work
146 demonstrated a decrease in hydrophobicity and charge of the *Salmonella* cell surface and a
147 corresponding change in envelope permeability in a *sfix* (*sanA*) mutant (57). Here, we
148 investigated the envelope permeability phenotypes caused by loss of SanA and found a
149 genetic interaction with ECA synthesis. Mutations expected to increase the availability of
150 Und-P caused the *sanA* mutant to become sensitive to SDS EDTA and cause activation of the
151 Rcs envelope stress response. We then selected suppressors of SDS EDTA sensitivity and
152 isolated partial loss of function mutations in *ftsI* (PBP3) and in *prc*, a protease involved in the
153 maturation of FtsI (58, 59), suggesting a role for cell division in this phenotype. Testing of
154 additional cell division mutations demonstrated that specifically loss of function in septal
155 PG synthesis but not divisome assembly suppressed the envelope permeability defect. Our
156 results tie the envelope permeability phenotype to Lipid II availability and support a model
157 in which SanA modulates the availability of Lipid II for septal PG synthesis. Furthermore, we
158 suggest that, when Lipid II levels are high such as during certain cellular stresses, FtsW and
159 FtsI activities can become unbalanced and that this leads to alteration of OM composition
160 and envelope permeability.

161

162 **RESULTS**

163 **Loss of SanA causes membrane permeability under cellular stress conditions.** We
164 began investigating SanA's role in envelope permeability by confirming previously published
165 phenotypes of SanA. We previously reported that a Δ*sanA* strain is sensitive to the detergent
166 SDS, as assayed by colony forming units (CFU) at 24 hours after treatment, when cells are
167 treated during stationary phase reached from carbon limitation (46). When we examined the
168 effect of Δ*sanA* on SDS sensitivity in carbon-limited stationary phase at shorter time scales,
169 we found that the decrease in CFU began within the first hour of treatment and continued

170 through 7 hours (**Figure 1A**). In contrast, wild-type cells maintained viability similar to that of
171 untreated cells throughout the 7-hour treatment. An insertion mutation in *sanA* has also
172 been reported to increase vancomycin sensitivity at high temperatures (43 °C), causing cells
173 to lyse at a concentration of vancomycin where wild-type cells can grow (55). To confirm this
174 in a Δ*sanA* mutant, we performed efficiency-of-plating assays (EOPs) with wild-type and
175 Δ*sanA* cells carrying either an empty vector or a low copy number plasmid expressing *sanA*.
176 When we treated cells with vancomycin and grew cultures at 43 °C, we found that the Δ*sanA*
177 strain was more sensitive to vancomycin and this phenotype could be complemented
178 (**Figure 1B**). To confirm this was a true change in resistance (i.e., the concentration of
179 antibiotic that can kill cells), we performed minimum inhibitory concentration (MIC) assays
180 and found that the MIC of vancomycin for the Δ*sanA* strain was significantly less than that of
181 wild type (**Figure 1C**).

182 Vancomycin is a large glycopeptide antibiotic for which entry into the cell is greatly impeded
183 by the OM (4, 60, 61) and anionic detergents such as SDS are excluded from the cell by the
184 strong hydrophilic network of lateral interactions between LPS molecules in the OM (1, 4).
185 Therefore, we examined the structure of the Lipid A component of LPS in the Δ*sanA* strain
186 under various growth conditions. We observed a large increase in hepta-acylated Lipid A in
187 the Δ*sanA* mutant when cells were grown in defined MOPS media with glucose but not when
188 the cells were grown at 37 or 43 °C in LB media (**Figure 1D, S1**). The hepta-acylated Lipid A
189 levels were returned to normal by plasmid-based complementation of *sanA*. Hepta-acylated
190 LPS is formed when PagP, an OMP, transfers a saturated acyl chain to LPS from a
191 phospholipid mislocalized to the outer leaflet of the OM (62). Thus, increased hepta-
192 acylated LPS is an indication of a loss of OM asymmetry causing increased phospholipids
193 on the cell surface (63). In support of this loss of asymmetry, overexpression of *pldA*, an outer
194 membrane phospholipase that removes an acyl chain from phospholipids mislocalized to
195 the outer membrane (64, 65), decreased the amount of hepta-acylated Lipid A in the Δ*sanA*
196 strain (**Figure 1D, S1**). However, *pldA* overexpression did not restore the Δ*sanA* mutant's
197 vancomycin resistance at 43 °C or SDS resistance during carbon limitation (**Figure S2**),

198 suggesting the loss of OM asymmetry is secondary to another defect that is causing OM
199 permeability.

200 SanA's effect on vancomycin resistance is only found at high temperatures (55) and *sanA* is
201 annotated to have a possible σ^H promoter (53, 54). Therefore, we investigated whether loss
202 of SanA affected heat shock resistance in carbon-limiting conditions. In fact, the Δ*sanA*
203 strain showed a small but significant decrease in survival at 57 °C compared to the wild-type
204 strain (**Figure 1E**). This increased sensitivity was not shared with deletion of the other gene
205 in *sanA*'s operon, *yeiS* (**Figure S3**). Overall, these data demonstrate that SanA is playing an
206 important role in maintaining the outer membrane permeability barrier specifically in
207 conditions of cellular stress such as carbon limitation or growth at high temperatures.

208 ***sanA* has genetic interactions with ECA mutations causing PG stress.** In investigating
209 how SanA affects membrane permeability, we made double mutants of *sanA* and non-
210 essential members of various envelope biosynthesis pathways. ECA is a component of the
211 Enterobacterales envelope and consists of a repeating, invariant trisaccharide unit that is
212 found surface exposed as the headgroup of a phospholipid or attached to LPS in place of O-
213 antigen, as well as cyclized in the periplasm (66). A paralog of *sanA*, *elyC*, has been shown
214 to have genetic interactions with enterobacterial common antigen (ECA) mutations (67) and
215 is involved in regulating the synthesis of one form of ECA (68). In addition, we identified
216 another gene, *yhdP*, which codes for a putative intermembrane phospholipid transporter
217 (47-50) in the same screen as *sanA*, and *yhdP*'s membrane permeability phenotypes are
218 dependent on the presence of ECA (46). Therefore, we decided to assay genetic interactions
219 between ECA biosynthesis genes and *sanA*.

220 We found that Δ*sanA* had a synthetic SDS EDTA sensitivity, even at 37 °C in LB media, when
221 paired with a deletion of *wecA*, the first gene in the ECA synthesis pathway (**Figure 2A**). EDTA
222 breaks the network of interactions between LPS molecules, increasing cells susceptibility to
223 SDS (69). Intriguingly, when we tested for genetic interactions between *sanA* and *wecE*,
224 which encodes a protein involved in synthesis of the third sugar in the ECA trisaccharide, we
225 found that Δ*wecE* causes SDS EDTA sensitivity and this sensitivity is suppressed by Δ*sanA*

226 (**Figure 2A**). These genetic interactions were apparent at 43 °C as well as 37 °C (**Figure S4A**)
227 and the synthetic SDS EDTA phenotype of the Δ*sanA* Δ*wecA* mutant could be complemented
228 with plasmid-based expression of *sanA* (**Figure S4B**). The difference in phenotype between
229 Δ*wecA* and Δ*wecE* suggested that it was not the loss of ECA that was important for the
230 phenotype but might instead be the interaction between ECA and other biosynthetic
231 pathways. Specifically, ECA synthesis uses the same isoprenoid carrier (Und-P) used for the
232 synthesis of PG (66). Therefore, we wondered if it might be PG synthesis stress caused by
233 sequestration of the isoprenoid carrier that is important for the genetic interaction with *sanA*.

234 We decided to compare the phenotypes of Δ*sanA* with deletion of the three
235 transglycosylases in the ECA synthesis pathway. The PG stress caused by deletion of each
236 subsequent transglycosylase is worse than the previous (34, 37, 67, 70). Δ*wecA* does not
237 cause apparent PG stress, Δ*wecG* causes minimal PG stress, and Δ*wecF* causes PG stress
238 as evidenced by envelope stress response activation, permeability defects, and cell shape
239 defects, although these defects are not as strong as those of Δ*wecE* (34, 37, 67, 70). When
240 we tested these mutants, we indeed found the Δ*sanA* Δ*wecA* strain showed the most SDS
241 EDTA sensitivity, while the Δ*sanA* Δ*wecG* strain showed a slight sensitivity and the Δ*sanA*
242 Δ*wecF* strain showed very similar SDS EDTA sensitivity to that of the Δ*sanA* strain (**Figure**
243 **2B**). These data show that, counterintuitively, the envelope permeability of a Δ*sanA* mutant
244 is increased by mutations that increase isoprenoid carrier availability.

245 ECA mutants causing PG stress have been shown to activate the Rcs (Regulator of Capsule
246 Synthesis) stress response, which directly responds to LPS defects but can also be activated
247 by PG stress (71-73). Therefore, we tested Rcs activation using a reporter assay with
248 luciferase genes driven by the *rprA* promoter (74, 75) in single and double deletion mutants
249 of *sanA*, *wecA* and *wecF*. Neither Δ*sanA* or Δ*wecA* caused Rcs activation alone (**Figure 2C**,
250 **S4C**); however, a Δ*sanA* Δ*wecA* mutant showed Rcs activation greater than that of the Δ*wecF*
251 or Δ*sanA* Δ*wecF* mutant. As these data and the SDS EDTA data point to interactions with
252 isoprenoid carrier availability and PG synthesis, we then assayed the cell shape of the Δ*sanA*
253 and Δ*wecA* single and double mutants. We grew cells for 7-10 generations in exponential
254 phase before the assay to ensure that cell shape was stable after exiting stationary phase

255 (76, 77). The aspect ratio (length/width) of all mutants was larger than wild type with the
256 Δ*sanA* Δ*wecA* mutant showing a significant shape change from that of the Δ*sanA* single
257 mutant (**Figure 2D**, **S4D**). Overall, these data demonstrate *sanA* has genetic interactions
258 causing increased permeability and envelope stress with increased isoprenoid carrier
259 availability.

260 **Spontaneous mutation to *ftsI* and *prc* suppress the Δ*sanA* Δ*wecA* SDS EDTA sensitivity.**
261 When assaying the SDS EDTA sensitivity of the Δ*sanA* Δ*wecA* double mutant, we
262 occasionally noticed the appearance of spontaneous suppressor mutants. Therefore, we
263 decided to select for these mutants to determine what types of mutations could suppress
264 the envelope permeability of this strain. We plated Δ*sanA* Δ*wecA* strain on a concentration
265 of SDS EDTA where it did not grow but the wild-type strain did and collected eleven
266 suppressor mutants from a total of 7 separate cultures. We grouped these mutants by their
267 antibiotic resistance patterns to find strains with similar mutations (**Figure S5**) and then
268 performed whole genome sequencing on representatives of each group, following up to
269 confirm that the mutations in the other mutants. These suppressor mutants each contained
270 one of four mutations, $ftsI_{V98E}$, $ftsI_{S165P}$, prc_{F365L}, or prc_{R578C} (**Figure 3A**). FtsI is the DD-
271 transpeptidase involved in septal PG synthesis during cell division (38, 78), while Prc (a.k.a.
272 Tsp) is a protease known to cleave FtsI's C terminal 11 amino acids to produce the fully
273 mature protein (58, 59). As Prc is necessary for FtsI maturation (58), we focused on the *ftsI*
274 mutations as the more direct suppressors. We linked the $ftsI_{V98E}$ mutation to a nearby Tn*10*
275 and used this marker to transfer the mutation to the wild-type, Δ*sanA*, Δ*wecA*, and Δ*sanA*
276 Δ*wecA* backgrounds. After being moved to a clean background, the $ftsI_{V98E}$ mutation
277 suppressed SDS EDTA sensitivity in the Δ*sanA* Δ*wecA* strain showing it was sufficient for
278 suppression (**Figure 3B**). We were not successful in moving the $ftsI_{S165P}$ mutation; however,
279 we used P1*vir* transduction to remove the mutations from the suppressor strain and this
280 prevented the SDS EDTA resistance of the suppressor strain (**Figure 3C**). Although we
281 assayed the effect of the $ftsI_{V98E}$ mutation on the vancomycin sensitivity of a Δ*sanA* strain at
282 43 °C, the $ftsI_{V98E}$ mutation caused vancomycin resistance in a wild-type background making

283 it difficult to assess whether its effect on the Δ*sanA* vancomycin sensitivity was specific
284 (**Figure S6**).

285 We then asked whether the *ftsI* mutations could suppress the Rcs activation found in the
286 Δ*sanA* Δ*wecA* strain. We found that the $ftsI_{S165P}$ mutation caused a growth delay and
287 maintained Rcs activation, while the $ftsI_{V98E}$ mutation brought Rcs activation in the Δ*sanA*
288 Δ*wecA* mutant back to nearly wild-type levels without a significant effect on growth (**Figure**
289 **3D**). We made an AlphaFold model (79) of a complex of FtsI, FtsW, FtsL, FtsB, and FtsQ,
290 which corresponds well to the crystal structure of this complex in *Pseudomonas aeruginosa*
291 (80), and mapped locations of the suppressor mutations onto this predicted structure
292 (**Figure 3E**). FtsI has two periplasmic domains, a pedestal domain thought to control
293 activation of FtsW and mediate interactions with FtsL and FtsB and the catalytic
294 transpeptidase domain (78, 81). The Prc cleavage site in FtsI is located in an unstructured
295 region adjacent to the transpeptidase domain, while the V98E and S165P mutations are
296 located in the pedestal domain (**Figure 3E**). Neither of these mutations has been previously
297 reported and their effect on FtsI activity is yet to be determined. Nevertheless, the consistent
298 and repeated isolation of mutations in *ftsI* and *prc* demonstrated that the envelope defect
299 leading to SDS EDTA sensitivity in the Δ*sanA* Δ*wecA* strain is related to the process of cell
300 division.

301 **Suppressor mutations in *ftsI* cause partial loss of function.** As the Δ*sanA* and Δ*sanA*
302 Δ*wecA* strains showed a cell shape with a higher aspect ratio than wild-type cells (**Figure**
303 **2D**) and the suppressor mutations we found are in cell division genes, we then assayed the
304 cell shape of the suppressor strains. Cells from both *ftsI* mutant strains were significantly
305 longer than the Δ*sanA* Δ*wecA* parent and had a greater aspect ratio (**Figure 4AB**). In contrast,
306 the aspect ratio of the *prc* mutants was indistinguishable from that of the Δ*sanA* Δ*wecA*
307 parent. The longer length of the *ftsI* mutants suggests that they have a partial loss of function
308 in their transpeptidase activity or in protein interactions. Therefore, we tested the
309 transpeptidase activity of the mutants through resistance to aztreonam, a β-lactam
310 antibiotic that this highly specific to FtsI (82).

311 As controls to show that activity of FtsI correlates to aztreonam resistance, we tested *ftsI23*
312 (Y281D), a temperature sensitive allele of *ftsI* that has reduced activity even at permissive
313 temperatures and can slow the rate of closure of the septum (83-85), and *ftsN*
314 overexpression which has been shown to result in increased activity of the divisome and to
315 suppress partial loss of function mutations in both divisome assembly and septal PG
316 synthesis (86-88). Given the temperature sensitive phenotype of *ftsI23,* we assayed
317 aztreonam MICs at both 30 and 37 °C. At 30 °C, *ftsN* overexpression caused a significant
318 increase in aztreonam MIC in the Δ*sanA* Δ*wecA* background (**Figure 4C**), while none of the
319 *ftsI* mutations caused a significant change in MIC. However, at 37 °C, *ftsI23* caused a
320 significant decrease in MIC and *ftsN* overexpression caused a significant increase
321 demonstrating that decreased *ftsI* activity correlates with decreased aztreonam resistance
322 and vice versa (**Figure 4C**). At this temperature, $ftsI_{V98E}$ caused a significant decrease in
323 aztreonam MIC compared to its Δ*sanA* Δ*wecA* parent, while $ftsI_{S165P}$ did not cause a
324 significant change. These data suggest that, while $ftsI_{V98E}$ has decreased transpeptidase
325 activity that may contribute to the longer cell shape, $ftsI_{S165P}$ does not have a severe effect
326 on transpeptidase activity. Therefore, the effect of these mutations on protein-protein
327 interactions, and more specifically FtsW activation, may be more important for
328 suppression.

329 To confirm that the *ftsI* mutations were loss-of-function mutations and to see whether their
330 suppression of the Δ*sanA* Δ*wecA* membrane permeability was unique, we tested the effect
331 of several gain- and loss-of-function mutations in divisome activity on the SDS EDTA
332 sensitivity of the Δ*sanA* Δ*wecA* strain. Our suppressor mutation, $ftsI_{V98E}$, suppressed the SDS
333 EDTA sensitivity of the Δ*sanA* Δ*wecA* strain when cells were grown at either 30 or 37 °C
334 (**Figure 4D**). However, *ftsI23* suppressed only at 30 °C, suggesting that there may be a range
335 of function loss for *ftsI* that can suppress envelope permeability. Neither *ftsA** (R286W) (89,
336 90) nor *ftsN* overexpression, both of which are activating mutations, suppressed the SDS
337 EDTA sensitivity of the Δ*sanA* Δ*wecA* mutant (**Figure 4D**). In fact, the SDS EDTA sensitivity of
338 the Δ*sanA* Δ*wecA* strain carrying the *ftsA** allele was greater than that of Δ*sanA* Δ*wecA* alone.
339 Overall, these data demonstrate that $ftsI_{V98E}$ and $ftsI_{S165P}$ are partial loss of function mutations

340 and that other loss of function mutations in *ftsI* can also suppress the Δ*sanA* Δ*wecA*
341 envelope permeability.

342 **Δ*sanA* Δ*wecA* envelope permeability is linked to septal PG synthesis.** As the SDS EDTA
343 sensitivity of the Δ*sanA* Δ*wecA* strain can be suppressed by mutations to *ftsI*, we next asked
344 whether SanA might influence the timing of assembly of the Z ring, which is the first step in
345 cell division. We expressed a GFP-version of FtsZ (91) and examined its localization in the
346 wild-type, Δ*sanA*, and Δ*sanA* $ftsI_{V98E}$ strains. However, we observed no difference in the
347 localization of FtsZ in these strains (**Figure 5**). Therefore, we decided to examine more cell
348 division mutations to determine whether divisome assembly and/or septal PG synthesis
349 were important for suppression of SDS EDTA sensitivity in the Δ*sanA* Δ*wecA* strain. We
350 examined the effect of three temperature sensitive loss-of-function mutations in divisome
351 assembly *ftsZ84* (G105S) (92), *ftsA12* (A188V) (93, 94), and *ftsA27* (S195P) (87, 95), as well
352 as a gain-of-function mutation, *ftsL** (E88K) (96, 97), and temperature sensitive loss-of-
353 function mutation in septal PG synthesis, *ftsQ1* (E125K) (93, 98). Given the temperature
354 sensitivity caused by these mutations we performed the experiment at 30 °C. None of the
355 mutations caused SDS EDTA sensitivity on their own at this temperature except *ftsQ1*, which
356 showed sensitivity similar to that of the Δ*sanA* Δ*wecA* strain (**Figure 6A**). However, only *ftsQ1*
357 suppressed the SDS EDTA sensitivity of the Δ*sanA* Δ*wecA* strain (**Figure 6B**), demonstrating
358 that these mutations can cross suppress. When we examined the effect of the mutations on
359 SDS EDTA sensitivity in a Δ*sanA* strain, we found that the *ftsZ84*, *ftsA12*, and *ftsL** mutations
360 cause SDS EDTA sensitivity in the Δ*sanA* background (**Figure 6C**). Overall, these data
361 demonstrate that the envelope permeability of the Δ*sanA* Δ*wecA* strain is suppressed by
362 slowing of septal PG synthesis and not by slowing of divisome assembly. Furthermore, our
363 data show that slowing divisome assembly can increase the envelope permeability of a
364 Δ*sanA* strain.

365 **Membrane permeability with loss of SanA is tied to Lipid II availability and FtsW activity.**
366 Our data show that partial loss of function mutations in septal PG synthesis can suppress
367 the Δ*sanA* Δ*wecA* strain's SDS EDTA sensitivity. As the spontaneous *ftsI* mutations we
368 isolated were in the FtsI pedestal domain that interacts with FtsW, we wondered whether

369 SanA's envelope permeability phenotypes relate to FtsW activity and what effect the *ftsI*
370 mutations we isolated have on this activity. A plasmid-based FtsW depletion strain has been
371 previously described (99) and we transferred the arabinose-inducible *ftsW* expressing
372 plasmid and chromosomal *ftsW* deletion to our strains. We then assayed growth and SDS
373 EDTA resistance with various concentrations of arabinose. When we examined SDS EDTA
374 resistance, we found that $ftsI_{V98E}$ could suppress the Δ*sanA* Δ*wecA* strain regardless of
375 arabinose concentration (**Figure 7A**). However, we also observed that $ftsI_{V98E}$ in a wild-type
376 background conferred resistance to arabinose depletion, allowing cells to grow at a lower
377 concentration of arabinose than is tolerated by the parent strain, suggesting increased
378 activity of FtsW (**Figure 7A**). We did not observe the same increase when $ftsI_{V98E}$ is expressed
379 in either the Δ*sanA* or Δ*sanA* Δ*wecA* background, suggesting that loss of SanA may increase
380 the activity of FtsW necessary for viability.

381 Given *sanA*'s genetic interaction with mutations altering isoprenoid carrier availability, we
382 further asked whether the availability of Lipid II, the substrate for PG synthesis, was involved
383 in SanA's envelope permeability phenotype. A chromosomal depletion strain for MurJ, the
384 Lipid II flippase (99, 100), where the promoter for *murJ* was replaced with the arabinose-
385 inducible P_{BAD} promoter has been described (100). We transduced this promoter into our
386 strains and assayed growth and SDS EDTA resistance at various arabinose concentrations.
387 Depletion of MurJ did not prevent suppression of Δ*sanA* Δ*wecA* SDS EDTA sensitivity by
388 $ftsI_{V98E}$ (**Figure 7B**). Therefore, we then decided to test the effect of overexpression of *murA*,
389 which is responsible for the first committed step in PG synthesis (101) and would be
390 expected to increase Lipid II levels. When we overexpressed *murA* in a Δ*sanA* strain, we
391 observed SDS EDTA sensitivity that phenocopied that observed in a Δ*sanA* Δ*wecA* strain and
392 this sensitivity could be suppressed by $ftsI_{V98E}$ (**Figure 7C**). Furthermore, overexpression of
393 *murA* decreased the level of SDS EDTA sensitivity suppression observed in a Δ*sanA* Δ*wecA*
394 strain. These data confirm that increased Lipid II availability leads to SDS EDTA sensitivity in
395 the absence of SanA and that this sensitivity can be suppressed through modulation of
396 septal PG synthesis.

397

398 **DISCUSSION**

399 Here, we set out to understand how SanA affects the cell's envelope permeability barrier. We
400 confirmed that a Δ*sanA* strain has envelope permeability phenotypes that occur under
401 cellular stress, such as carbon limitation and high temperatures. Additionally, we discovered
402 that a Δ*sanA* Δ*wecA* strain, which has heightened isoprenoid carrier levels due to a lack of
403 ECA synthesis (37), had a pronounced, synthetic SDS EDTA sensitivity and that this
404 sensitivity could be suppressed by partial loss of function mutations to either *ftsI* or to *prc*.
405 When investigating the suppression phenotype, we found that mutations resulting in partial
406 loss of function for septal PG synthesis, but not early divisome assembly, could suppress
407 the Δ*sanA* Δ*wecA* SDS EDTA sensitivity. Moreover, we observed that overexpressing *murA* in
408 a Δ*sanA* strain phenocopied Δ*sanA* Δ*wecA*, indicating increased Lipid II is important for the
409 SDS EDTA phenotype. Finally, the *ftsI* mutations we identified were located in the pedestal
410 domain of FtsI important for protein-protein interactions, and at least one of the mutations,
411 $ftsI_{V98E}$, increases FtsW activity, highlighting the importance of the FtsI-FtsW interaction for
412 this phenotype.

413 Based on these findings, we propose a model which provides a parsimonious explanation
414 for our results. In this model, we reason that, under certain cellular stress conditions, the
415 amount of Lipid II available for septal PG synthesis increases. For example, enzymes
416 involved in Lipid II synthesis might have higher activity rates at higher temperature leading to
417 increased Lipid II synthesis. Alternatively, under carbon limited conditions, decreased cell
418 elongation and the lower surface area of stationary phase cells could lead to higher Lipid II
419 levels available for septal PG synthesis. The increase in substrate availability for septal PG
420 synthesis creates an imbalance of FtsI and FtsW activity, with FtsI activity increasing more
421 than FtsW activity. This imbalance ultimately leads to envelope permeability. This model
422 would also suggest that loss-of-function mutations in early divisome assembly increase the
423 membrane permeability of a Δ*sanA* strain by decreasing the number of active septal PG
424 synthesis complexes and so increasing the ratio of Lipid II to active septal PG synthesis
425 complexes. SanA restores this balance by limiting the amount of Lipid II available for septal

426 PG synthesis. In SanA's absence, mutations that reduce FtsI activity and, in at least in some
427 cases, increase FtsW activity, can restore this balance even when excess Lipid II is present.

428 In support of this model, a paper (102) was published while this manuscript was in
429 preparation that identified a suppressive phenotype of Δ*sanA* for the growth of several cell
430 division mutants including *ftsI23* and found that PG incorporation was increased in a Δ*sanA*
431 strain (102). Although the paper examined different conditions from our study, it also found
432 synthetic interactions between early genes in ECA synthesis and Δ*sanA*, specifically for
433 growth in low osmolarity (102). From these findings it was unclear whether SanA's
434 phenotypes related to septal PG synthesis or PG synthesis more broadly. However, our work
435 clearly demonstrates that the membrane permeability phenotype which occurs when Lipid
436 II levels are increased coupled with the absence of SanA, specifically relates to septal PG
437 synthesis and that changes to the elongasome (involved in cell lengthening) are not
438 necessary to prevent permeability.

439 How SanA alters Lipid II availability for septal PG synthesis remains an unanswered
440 question. The recent paper speculates that SanA may have enzymatic activity, based on
441 phenotypes of *sanA* point mutations (102). We agree that predicted structures of SanA
442 suggest it has enzymatic activity, and we have made similar point mutations. However, many
443 of these mutants did not produce a stable protein, making it difficult to confirm enzymatic
444 activity. Nevertheless, if SanA does have enzymatic activity, it is possible that it alters or
445 degrades Lipid II in some way that promotes its recycling. Alternatively, it is possible that
446 SanA binds to and sequesters Lipid II. However, the number of SanA molecules in the cell
447 are 10 to 50-fold less than those of Lipid II under normal growth conditions (103, 104). Thus,
448 a significant increase in SanA levels under activating conditions would be necessary for this
449 possibility to occur. The synthesis of Lipid II has been found to be regulated through the
450 dimerization of MraY which binds to excess Lipid II, inhibiting its activity and Lipid II synthesis
451 (105). Given this, it is possible SanA is involved in this regulatory pathway. However, it's
452 perhaps more likely that SanA directly controls the availability of Lipid II for septal PG
453 synthesis rather than overall Lipid II levels. For instance, SanA could feed Lipid II to FtsW in
454 some manner that ensures correct substrate availability to balance FtsI and FtsW levels.

455 This idea fits well with the slight increase in cell length observed in the Δ*sanA* strain, which
456 suggests that cells are elongating longer before they divide. However, differentiating these
457 possibilities will require future investigation.

458 FtsI's cytoplasmic region and transmembrane helix are important for its recruitment to the
459 Z-ring through interaction with FtsW (78). The periplasmic portion of FtsI contains the
460 pedestal domain, which is important for interacting with other members of the septal PG
461 synthesis complex, and the catalytic domain that acts as the transpeptidase during septal
462 PG synthesis (78). Both FtsI variants that we identified, $FtsI^{V98E}$ and $FtsI^{S165P}$, are in the
463 pedestal domain of FtsI. Notably, this domain is proposed to recruit FtsN (the final activating
464 protein for the complex), to interact with FtsW (the transglycosylase) and to control its
465 activation, and to control FtsI transpeptidase activity (78, 81, 106). It is interesting then that
466 although both $FtsI^{V98E}$ and $FtsI^{S165P}$ resulted in longer cells, suggesting a partial loss-of-
467 function, $FtsI^{V98E}$ also made wild type cells resistant to FtsW depletion, suggesting increased
468 FtsW activation. Thus, these mutations may be affecting the activity of both FtsI and FtsW—
469 and in differing directions. Mutations to residues near S165 (R166 and R167) have been
470 shown to either cause constitutive activation of FtsW or loss-of-function in FtsI
471 transpeptidase activity so it may be that S165P causes functional changes to both FtsI and
472 FtsW as well. Further investigation of these mutants may lead to greater insight into the
473 complex regulatory interactions carried out by the pedestal domain of FtsI.

474 Finally, it is worth considering how an imbalance in septal PG synthesis, particularly FtsI and
475 FtsW activities, leads to increased envelope permeability. The synthesis of PG and OM
476 components share many precursors. Therefore, it is possible that an increase in septal PG
477 synthesis could limit some OM components, hindering proper OM synthesis. However, our
478 cell length data do not support increased septal PG synthesis in either a Δ*sanA* or Δ*sanA*
479 Δ*wecA* strain. Thus, we find it more likely that the envelope biosynthesis phenotype is due to
480 a lack of coordination between different envelope biosynthetic pathways. For instance, OMP
481 biosynthesis has been shown to increase in the presence of immature PG (45). Therefore, it
482 is possible that the imbalance between FtsI and FtsW activity leads to an increase in the
483 formation of immature PG, causing excess OMP insertion near the septum. Finally, it is

484 possible that there is a defect in OM invagination caused by the alteration in septal PG
485 synthesis. These questions will be interesting avenues for future investigations.

486

487 **MATERIALS AND METHODS**

488 **Strains and growth conditions.** All strains used in this study are listed in **Table S1**. Cultures
489 were inoculated and grown at 37°C unless otherwise noted in LB, M63 or MOPS media.
490 Cultures were supplemented with 20mg/liter chloramphenicol, 25mg/liter kanamycin,
491 10mg/liter tetracycline, or a combination thereof as necessary. M63 was supplemented with
492 1mM $MgSO_4$, 0.2% glucose, 50mg/ml thiamine, and 2% arabinose. Carbon-limited cultures
493 were grown in M63 medium supplemented with 0.05% glucose. Keio insertion-deletion
494 mutations and other indicted mutations were moved using P1*vir* transduction (107).
495 Antibiotic resistance cassettes were removed with the Flp recombinase-FRT system as
496 described previously described (108). To clone a plasmid encoding *sanA*, genomic DNA was
497 amplified using the primers pZS21-RBS-*sanA* F and *sanA*-pZS21 R (**Table S2**). pZS21 (109)
498 was amplified using pZS21 F and pZS21-RBS R (**Table S2**). The fragments were assembled
499 using HiFi Assembly Master Mix (New England Biolab) as per the manufacturer's
500 instructions.

501 **Sensitivity assays.** Resistance to SDS in stationary phase was assay as we have previously
502 described (46). For EOPs, overnight cultures were serially diluted as indicated, plated on the
503 indicated plates, and plates were incubated overnight. For Kirby-Bauer tests, 100 µL of
504 overnight cultures were then added to 3 mL liquified top LB agar and spread on LB agar
505 plates. Preconditioned antibiotic disks were placed on the agar surface and plates were
506 incubated overnight. The diameter of the zone of clearance was measured in at least two
507 directions. For MICs, overnight cultures were normalized to an OD_{600} of 0.1 then further
508 diluted 1:1000. Diluted cultures were then added to 96-well plate followed by two-fold
509 dilutions of the indicated antibiotic. Plates were incubated at 37 °C overnight. Then, OD_{600}
510 was read using a BioTek Synergy H1 plate reader. The lowest concentration where growth is
511 inhibited was determined to be the MIC.

512 **Lipid A modification assay.** Cultures were grown overnight in the indicated media. Cells
513 were then diluted 1:100 in fresh medium containing 2.5 µCi/mL of ^{32}P and grown to OD_{600} 0.6-
514 0.8. LPS was purified and mid-acid hydrolysis was used to liberate Lipid A which was
515 visualized using thin-layer chromatography (TLC) as has been previously described (110).

516 **Suppressor isolation.** To isolate suppressors, cultures of the Δ*sanA* Δ*wecA* strain were
517 serial diluted and plated with 0.5% SDS with 1.0 or 1.1 mM EDTA. Colonies that grew were
518 isolated and suppression was confirmed by EOP. Verified suppressors were categorized
519 based on antibiotic resistance profiles. For a representative of each category and the parent
520 strain, genomic DNA was purified using the DNeasy Blood and Tissue Kit (Qiagen) and
521 provided to SeqCoast Genomics for library preparation and sequencing. Briefly, libraries
522 were prepared using a DNA Prep Tagmentation Kit (Illumina) and unique dual indexes.
523 Sequencing was performed with an Illumina NextSeq2000 using a 300-cycle flow cell
524 producing 2x150bp reads. A PhiX control was used to optimize base calling. Demultiplexing,
525 read trimming, and run analytics were performed using DRAGEN software version. SeqCoast
526 quality trimmed the reads, mapped them to the MG1655 reference genome (Genebank ID
527 U00096.3) and called variants using Trimmomatic and Breseq software (111-113). The
528 identified mutations were confirmed in all suppressors using Sanger sequencing.
529 Suppressors strains were linked to a tetracycline marking using P1*vir* transduction of the *zab*-
530 3051:Tn*10* insertion site (114).

531 **P_{rprA} reporter activity assay.** Overnight cultures carrying the pJW15-P_{rprA} reporter plasmid
532 (74, 75) were assayed for luciferase activity as has been previously described (68). Data are
533 representative of three biological replicates, each performed in technical triplicate.

534 **Cell imaging and analysis.** Overnight cultures were diluted 1:10,000 and grown to an OD_{600}
535 ~0.5 before imaging. Imaging and cell shape analysis were performed as previously
536 described (115, 116). Briefly, 5-10 µl of culture were added to a 0.8% agarose gel pad
537 supplemented with 8 mM $MgSO_4$. Differential interference contrast (DIC) images were
538 captured using an Andor iXon Ultra 897 EMCCD camera (effective pixel size 160 nm) on an
539 inverted Nikon Eclipse-Ti™ microscope with a 100× 1.49 NA TIRF objective. Cell length and

540 width was determined using a MATLAB (MathWorks, Inc) script (115). Raincloud plots were
541 made and statistics calculated using Raincloud-shiny (117). For protein localization,
542 overnight cultures were diluted to OD_{600} 0.1 and grown to OD_{600} 0.4. GFP-tagged proteins
543 were excited by a 488 nm laser. GFP-tagged *ftsZ* was expressed from pXY027 (91) (Addgene
544 #98915). Demographs were constructed using ImageJ plug-in MicrobeJ (118). Cells were
545 aligned at mid-cell and sorted by their length, and fluorescence intensity was normalized.

546

547 **ACKNOWLEDGEMENTS**

548 Thank you to the current and former members of the Mitchell Lab as well as Drs. Jolene
549 Ramsey, Jennifer Herman, Deborah Siegele, Ryland Young (Texas A&M University), Anna
550 Konovalova (University of Texas Health Science Center Houston), Petra Levin (Washington
551 University in St. Louis), and Natividad Ruiz (The Ohio State University) for insights and
552 productive discussions. Thank you to Dr. Srutha Venkatesan for helping with the initial stages
553 of the cell-length experiments. We would also like to thank Dr. Thomas Silhavy (Princeton
554 University) for all his assistance with the early stages of this project. Thank you to Drs. Petra
555 Levin (Washington University in St. Louis), Natividad Ruiz (The Ohio State University), and
556 Thomas Bernhardt (Harvard University Medical School) for sharing strains with us to
557 facilitate these experiments and to Dr. Tracy Raivio (University of Alberta) for providing the
558 pJW15-P_{rpra} reporter plasmid and Dr. Jie Xiao (Johns Hopkins University School of Medicine)
559 for providing pXY027 (Addgene #98915).

560 This work was supported by the National Institute of Allergy and Infectious Diseases under
561 award number R01-AI155915 (to A.M.M.) and the National Institute of General Medical
562 Sciences under award number R01-GM129000 (to B.N.).

563

564 **REFERENCES**

565 1. Silhavy TJ, Kahne D, Walker S. 2010. The bacterial cell envelope. Cold Spring Harbor
566 Perspectives in Biology 2.

2. Braun V. 1975. Covalent lipoprotein from the outer membrane of *Escherichia coli*. Biochimica et Biophysica Acta (BBA) - Reviews on Biomembranes 415:335-377.
3. Park JS, Lee WC, Yeo KJ, Ryu K-S, Kumarasiri M, Hesek D, Lee M, Mobashery S, Song JH, Kim SI, Lee JC, Cheong C, Jeon YH, Kim H-Y. 2012. Mechanism of anchoring of OmpA protein to the cell wall peptidoglycan of the gram-negative bacterial outer membrane. The FASEB Journal 26:219-228.
4. Nikaido H. 2003. Molecular basis of bacterial outer membrane permeability revisited. Microbiology and Molecular Biology Reviews 67:593-656.
5. Henderson JC, Zimmerman SM, Crofts AA, Boll JM, Kuhns LG, Herrera CM, Trent MS. 2016. The power of asymmetry: Architecture and assembly of the Gram-negative outer membrane lipid bilayer. Annual Review of Microbiology 70:255-278.
6. Berry J, Rajaure M, Pang T, Young R. 2012. The spanin complex is essential for lambda lysis. J Bacteriol 194:5667-74.
7. Rojas ER, Billings G, Odermatt PD, Auer GK, Zhu L, Miguel A, Chang F, Weibel DB, Theriot JA, Huang KC. 2018. The outer membrane is an essential load-bearing element in Gram-negative bacteria. Nature 559:617-621.
8. Navarro Llorens JM, Tormo A, Martinez-Garcia E. 2010. Stationary phase in gram-negative bacteria. FEMS Microbiol Rev 34:476-95.
9. MacNair CR, Brown ED. 2020. Outer membrane disruption overcomes intrinsic, acquired, and spontaneous antibiotic resistance. mBio 11:e01615-20.
10. Lehman KM, Grabowicz M. 2019. Countering gram-negative antibiotic resistance: Recent progress in disrupting the outer membrane with novel therapeutics. Antibiotics 8:163.
11. Vetterli SU, Zerbe K, Müller M, Urfer M, Mondal M, Wang S-Y, Moehle K, Zerbe O, Vitale A, Pessi G, Eberl L, Wollscheid B, Robinson JA. 2018. Thanatin targets the intermembrane protein complex required for lipopolysaccharide transport in *Escherichia coli*. Science Advances 4:eaau2634.
12. Srinivas N, Jetter P, Ueberbacher BJ, Werneburg M, Zerbe K, Steinmann J, Van der Meijden B, Bernardini F, Lederer A, Dias RLA, Misson PE, Henze H, Zumbrunn J,

596 Gombert FO, Obrecht D, Hunziker P, Schauer S, Ziegler U, Käch A, Eberl L, Riedel K,
597 DeMarco SJ, Robinson JA. 2010. Peptidomimetic Antibiotics Target Outer-Membrane
598 Biogenesis in *Pseudomonas aeruginosa*. Science 327:1010-1013.
599 13. Steenhuis M, Abdallah AM, de Munnik SM, Kuhne S, Sterk G-J, van den Berg van
600 Saparoea B, Westerhausen S, Wagner S, van der Wel NN, Wijtmans M, van Ulsen P,
601 Jong WSP, Luirink J. Inhibition of autotransporter biogenesis by small molecules.
602 Molecular Microbiology 0.
603 14. Storek KM, Auerbach MR, Shi H, Garcia NK, Sun D, Nickerson NN, Vij R, Lin Z,
604 Chiang N, Schneider K, Wecksler AT, Skippington E, Nakamura G, Seshasayee D,
605 Koerber JT, Payandeh J, Smith PA, Rutherford ST. 2018. Monoclonal antibody
606 targeting the β-barrel assembly machine of *Escherichia coli* is bactericidal.
607 Proceedings of the National Academy of Sciences 115:3692-3697.
608 15. Hart EM, Mitchell AM, Konovalova A, Grabowicz M, Sheng J, Han X, Rodriguez-Rivera
609 FP, Schwaid AG, Malinverni JC, Balibar CJ, Bodea S, Si Q, Wang H, Homsher MF,
610 Painter RE, Ogawa AK, Sutterlin H, Roemer T, Black TA, Rothman DM, Walker SS,
611 Silhavy TJ. 2019. A small-molecule inhibitor of BamA impervious to efflux and the
612 outer membrane permeability barrier. Proc Natl Acad Sci U S A 116:21748-21757.
613 16. Urfer M, Bogdanovic J, Lo Monte F, Moehle K, Zerbe K, Omasits U, Ahrens CH, Pessi
614 G, Eberl L, Robinson JA. 2016. A peptidomimetic antibiotic targets outer membrane
615 proteins and disrupts selectively the outer membrane in *Escherichia coli*. Journal of
616 Biological Chemistry 291:1921-1932.
617 17. Steenhuis M, Corona F, ten Hagen-Jongman CM, Vollmer W, Lambin D, Selhorst P,
618 Klaassen H, Versele M, Chaltin P, Luirink J. 2021. Combining cell envelope stress
619 reporter assays in a screening approach to identify BAM complex inhibitors. ACS
620 Infectious Diseases 7:2250-2263.
621 18. Konovalova A, Kahne DE, Silhavy TJ. 2017. Outer Membrane Biogenesis. Annu Rev
622 Microbiol 71:539-556.
623 19. Garde S, Chodisetti Pavan K, Reddy M. 2021. Peptidoglycan: Structure, Synthesis,
624 and Regulation. EcoSal Plus 9.

625 20. May KL, Silhavy TJ. 2017. Making a membrane on the other side of the wall.
626 Biochimica et Biophysica Acta (BBA) - Molecular and Cell Biology of Lipids
627 1862:1386-1393.
628 21. John E. Cronan J, Rock CO. 2008. Biosynthesis of membrane lipids. EcoSal Plus 3.
629 22. Fivenson EM, Dubois L, Bernhardt TG. 2024. Co-ordinated assembly of the
630 multilayered cell envelope of Gram-negative bacteria. Current Opinion in
631 Microbiology 79:102479.
632 23. Rodionov DG, Ishiguro EE. 1996. Dependence of peptidoglycan metabolism on
633 phospholipid synthesis during growth of *Escherichia coli*. Microbiology (Reading)
634 142 (Pt 10):2871-7.
635 24. Som N, Reddy M. 2023. Cross-talk between phospholipid synthesis and
636 peptidoglycan expansion by a cell wall hydrolase. Proceedings of the National
637 Academy of Sciences 120:e2300784120.
638 25. Oldewurtel ER, Kitahara Y, Cordier B, Wheeler R, Özbaykal G, Brambilla E, Boneca
639 IG, Renner LD, van Teeffelen S. 2023. Cell envelope growth of Gram-negative
640 bacteria proceeds independently of cell wall synthesis. Embo j 42:e112168.
641 26. Fivenson EM, Rohs PDA, Vettiger A, Sardis MF, Torres G, Forchoh A, Bernhardt TG.
642 2023. A role for the Gram-negative outer membrane in bacterial shape
643 determination. Proceedings of the National Academy of Sciences
644 120:e2301987120.
645 27. Goodall ECA, Isom GL, Rooke JL, Pullela K, Icke C, Yang Z, Boelter G, Jones A,
646 Warner I, Da Costa R, Zhang B, Rae J, Tan WB, Winkle M, Delhaye A, Heinz E, Collet
647 J-F, Cunningham AF, Blaskovich MA, Parton RG, Cole JA, Banzhaf M, Chng S-S,
648 Vollmer W, Bryant JA, Henderson IR. 2021. Loss of YhcB results in dysregulation of
649 coordinated peptidoglycan, LPS and phospholipid synthesis during *Escherichia coli*
650 cell growth. PLOS Genetics 17:e1009586.
651 28. Li G, Hamamoto K, Kitakawa M. 2012. Inner Membrane Protein YhcB Interacts with
652 RodZ Involved in Cell Shape Maintenance in *Escherichia coli*. ISRN Mol Biol
653 2012:304021.

654 29. Wieczorek A, Sendobra A, Maniyeri A, Sugalska M, Klein G, Raina S. 2022. A New
655 Factor LapD Is Required for the Regulation of LpxC Amounts and
656 Lipopolysaccharide Trafficking. Int J Mol Sci 23.
657 30. Hummels KR, Berry SP, Li Z, Taguchi A, Min JK, Walker S, Marks DS, Bernhardt TG.
658 2023. Coordination of bacterial cell wall and outer membrane biosynthesis. Nature
659 615:300-304.
660 31. Rick PD, Hubbard GL, Barr K. 1994. Role of the *rfe* gene in the synthesis of the O8
661 antigen in *Escherichia coli* K-12. Journal of Bacteriology 176:2877-2884.
662 32. Klena JD, Schnaitman CA. 1993. Function of the *rfb* gene cluster and the *rfe* gene in
663 the synthesis of O antigen by *Shigella dysenteriae* 1. Molecular Microbiology 9:393-
664 402.
665 33. Alexander DC, Valvano MA. 1994. Role of the rfe gene in the biosynthesis of the
666 *Escherichia coli* O7-specific lipopolysaccharide and other O-specific
667 polysaccharides containing N-acetylglucosamine. Journal of Bacteriology
668 176:7079-7084.
669 34. Danese PN, Oliver GR, Barr K, Bowman GD, Rick PD, Silhavy TJ. 1998. Accumulation
670 of the enterobacterial common antigen lipid II biosynthetic intermediate stimulates
671 *degP* transcription in *Escherichia coli*. Journal of Bacteriology 180:5875-5884.
672 35. Jorgenson MA, Kannan S, Laubacher ME, Young KD. 2016. Dead-end intermediates
673 in the enterobacterial common antigen pathway induce morphological defects in
674 *Escherichia coli* by competing for undecaprenyl phosphate. Molecular Microbiology
675 100:1-14.
676 36. Castelli ME, Véscovi EG. 2011. The Rcs signal transduction pathway is triggered by
677 enterobacterial common antigen structure alterations in *Serratia marcescens*.
678 Journal of Bacteriology 193:63-74.
679 37. Eade CR, Wallen TW, Gates CE, Oliverio CL, Scarbrough BA, Reid AJ, Jorgenson MA,
680 Young KD, Troutman JM. 2021. Making the enterobacterial common antigen glycan
681 and measuring its substrate sequestration. ACS Chem Biol 16:691-700.

682 38. Cameron TA, Margolin W. 2024. Insights into the assembly and regulation of the
683 bacterial divisome. Nature Reviews Microbiology 22:33-45.
684 39. Levin Petra A, Janakiraman A. 2021. Localization, Assembly, and Activation of the
685 *Escherichia coli* Cell Division Machinery. EcoSal Plus 9:eESP-0022-2021.
686 40. Gray AN, Egan AJF, van't Veer IL, Verheul J, Colavin A, Koumoutsi A, Biboy J, Altelaar
687 AFM, Damen MJ, Huang KC, Simorre J-P, Breukink E, den Blaauwen T, Typas A, Gross
688 CA, Vollmer W. 2015. Coordination of peptidoglycan synthesis and outer membrane
689 constriction during *Escherichia coli* cell division. eLife 4:e07118.
690 41. Szczepaniak J, Holmes P, Rajasekar K, Kaminska R, Samsudin F, Inns PG, Rassam P,
691 Khalid S, Murray SM, Redfield C, Kleanthous C. 2020. The lipoprotein Pal stabilises
692 the bacterial outer membrane during constriction by a mobilisation-and-capture
693 mechanism. Nature Communications 11:1305.
694 42. Gerding MA, Ogata Y, Pecora ND, Niki H, De Boer PAJ. 2007. The trans-envelope Tol–
695 Pal complex is part of the cell division machinery and required for proper outer-
696 membrane invagination during cell constriction in *E. coli*. Molecular Microbiology
697 63:1008-1025.
698 43. Tsang M-J, Yakhnina AA, Bernhardt TG. 2017. NlpD links cell wall remodeling and
699 outer membrane invagination during cytokinesis in *Escherichia coli*. PLOS Genetics
700 13:e1006888.
701 44. Yakhnina AA, Bernhardt TG. 2020. The Tol-Pal system is required for peptidoglycan-
702 cleaving enzymes to complete bacterial cell division. Proceedings of the National
703 Academy of Sciences 117:6777-6783.
704 45. Mamou G, Corona F, Cohen-Khait R, Housden NG, Yeung V, Sun D, Sridhar P, Pazos
705 M, Knowles TJ, Kleanthous C, Vollmer W. 2022. Peptidoglycan maturation controls
706 outer membrane protein assembly. Nature 606:953-959.
707 46. Mitchell AM, Wang W, Silhavy TJ. 2017. Novel Rpos-dependent mechanisms
708 strengthen the envelope permeability barrier during stationary phase. J Bacteriol
709 199:e00708-16.

710 47. Grimm J, Shi H, Wang W, Mitchell AM, Wingreen NS, Huang KC, Silhavy TJ. 2020. The
711 inner membrane protein YhdP modulates the rate of anterograde phospholipid flow
712 in *Escherichia coli*. Proc Natl Acad Sci U S A 117:26907-26914.
713 48. Ruiz N, Davis RM, Kumar S. 2021. YhdP, TamB, and YdbH are redundant but essential
714 for growth and lipid homeostasis of the gram-negative outer membrane. mBio
715 12:e02714-21.
716 49. Douglass MV, McLean AB, Trent MS. 2022. Absence of YhdP, TamB, and YdbH leads
717 to defects in glycerophospholipid transport and cell morphology in Gram-negative
718 bacteria. PLOS Genetics 18:e1010096.
719 50. Rai AK, Sawasato K, Bennett HC, Kozlova A, Sparagna GC, Bogdanov M, Mitchell AM.
720 2024. Genetic evidence for functional diversification of gram-negative
721 intermembrane phospholipid transporters. PLOS Genetics 20:e1011335.
722 51. Mitchell AM, Srikumar T, Silhavy TJ. 2018. Cyclic enterobacterial common antigen
723 maintains the outer membrane permeability barrier of *Escherichia coli* in a manner
724 controlled by Yhdp. mBio 9:e01321-18.
725 52. van Heijenoort J. 2011. Peptidoglycan hydrolases of Escherichia coli. Microbiol Mol
726 Biol Rev 75:636-63.
727 53. Karp PD, Ong WK, Paley S, Billington R, Caspi R, Fulcher C, Kothari A,
728 Krummenacker M, Latendresse M, Midford PE, Subhraveti P, Gama-Castro S, Muñiz-
729 Rascado L, Bonavides-Martinez C, Santos-Zavaleta A, Mackie A, Collado-Vides J,
730 Keseler IM, Paulsen I. 2018. The EcoCyc database. EcoSal Plus
731 8:10.1128/ecosalplus.ESP-0006-2018.
732 54. Keseler IM, Mackie A, Santos-Zavaleta A, Billington R, Bonavides-Martínez C, Caspi
733 R, Fulcher C, Gama-Castro S, Kothari A, Krummenacker M, Latendresse M, Muñiz-
734 Rascado L, Ong Q, Paley S, Peralta-Gil M, Subhraveti P, Velázquez-Ramírez DA,
735 Weaver D, Collado-Vides J, Paulsen I, Karp PD. 2016. The EcoCyc database:
736 reflecting new knowledge about *Escherichia coli* K-12. Nucleic Acids Research
737 45:D543-D550.

738 55. Rida S, Caillet J, Alix JH. 1996. Amplification of a novel gene, sanA, abolishes a
739 vancomycin-sensitive defect in *Escherichia coli*. Journal of Bacteriology 178:94-102.
740 56. Mouslim C, Cano AD, Casadesús J. 1998. The sfiX, rfe and metN genes of
741 *Salmonella typhimurium* and their involvement in the Hisc pleiotropic response.
742 Molecular and General Genetics MGG 259:46-53.
743 57. Aleksandrowicz A, Kolenda R, Baraniewicz K, Thurston TLM, Suchański J, Grzymajlo
744 K. 2024. Membrane properties modulation by SanA: implications for xenobiotic
745 resistance in *Salmonella* Typhimurium. Frontiers in Microbiology 14.
746 58. Hara H, Nishimura Y, Kato J, Suzuki H, Nagasawa H, Suzuki A, Hirota Y. 1989.
747 Genetic analyses of processing involving C-terminal cleavage in penicillin-binding
748 protein 3 of *Escherichia coli*. J Bacteriol 171:5882-9.
749 59. Chueh CK, Som N, Ke LC, Ho MR, Reddy M, Chang CI. 2019. Structural Basis for the
750 Differential Regulatory Roles of the PDZ Domain in C-Terminal Processing
751 Proteases. mBio 10.
752 60. Ruiz N, Falcone B, Kahne D, Silhavy TJ. 2005. Chemical conditionality: a genetic
753 strategy to probe organelle assembly. Cell 121:307-17.
754 61. Wu T, Malinverni J, Ruiz N, Kim S, Silhavy TJ, Kahne D. 2005. Identification of a
755 multicomponent complex required for outer membrane biogenesis in *Escherichia*
756 *coli*. Cell 121:235-45.
757 62. Bishop RE, Gibbons HS, Guina T, Trent MS, Miller SI, Raetz CR. 2000. Transfer of
758 palmitate from phospholipids to lipid A in outer membranes of gram-negative
759 bacteria. Embo j 19:5071-80.
760 63. Jia W, Zoeiby AE, Petruzziello TN, Jayabalasingham B, Seyedirashti S, Bishop RE.
761 2004. Lipid trafficking controls endotoxin acylation in outer membranes of
762 *Escherichia coli*. Journal of Biological Chemistry 279:44966-44975.
763 64. Niek D. 2000. Outer-membrane phospholipase A: known structure, unknown
764 biological function. Molecular Microbiology 35:711-717.

765 65. Malinverni JC, Silhavy TJ. 2009. An ABC transport system that maintains lipid
766 asymmetry in the Gram-negative outer membrane. Proceedings of the National
767 Academy of Sciences 106:8009-8014.
768 66. Rai AK, Mitchell AM. 2020. Enterobacterial common antigen: Synthesis and function
769 of an enigmatic molecule. mBio 11:e01914-20.
770 67. Paradis-Bleau C, Kritikos G, Orlova K, Typas A, Bernhardt TG. 2014. A genome-wide
771 screen for bacterial envelope biogenesis mutants identifies a novel factor involved
772 in cell wall precursor metabolism. PLoS Genet 10:e1004056.
773 68. Rai AK, Carr JF, Bautista DE, Wang W, Mitchell AM. 2021. ElyC and cyclic
774 enterobacterial common antigen regulate synthesis of phosphoglyceride-linked
775 enterobacterial common antigen. mBio 12:e02846-21.
776 69. Marvin HJ, ter Beest MB, Witholt B. 1989. Release of outer membrane fragments
777 from wild-type *Escherichia coli* and from several *E. coli* lipopolysaccharide mutants
778 by EDTA and heat shock treatments. Journal of bacteriology 171:5262-5267.
779 70. Jorgenson MA, Kannan S, Laubacher ME, Young KD. 2016. Dead-end intermediates
780 in the enterobacterial common antigen pathway induce morphological defects in
781 *Escherichia coli* by competing for undecaprenyl phosphate. Mol Microbiol 100:1-14.
782 71. Konovalova A, Mitchell AM, Silhavy TJ. 2016. A lipoprotein/beta-barrel complex
783 monitors lipopolysaccharide integrity transducing information across the outer
784 membrane. Elife 5:e15276.
785 72. Wall E, Majdalani N, Gottesman S. 2018. The Complex Rcs Regulatory Cascade.
786 Annual Review of Microbiology 72:111-139.
787 73. Tata M, Kumar S, Lach SR, Saha S, Hart EM, Konovalova A. 2021. High-throughput
788 suppressor screen demonstrates that RcsF monitors outer membrane integrity and
789 not Bam complex function. Proceedings of the National Academy of Sciences
790 118:e2100369118.
791 74. Macritchie DM, Ward JD, Nevesinjac AZ, Raivio TL. 2008. Activation of the Cpx
792 envelope stress response down-regulates expression of several locus of enterocyte

effacement-encoded genes in enteropathogenic Escherichia coli. Infect Immun 76:1465-75.

75. Wong JL, Vogt SL, Raivio TL. 2013. Using reporter genes and the *Escherichia coli* ASKA overexpression library in screens for regulators of the Gram negative envelope stress response. Methods Mol Biol 966:337-57.

76. Santos JM, Freire P, Vicente M, Arraiano CM. 1999. The stationary-phase morphogene bolA from *Escherichia coli* is induced by stress during early stages of growth. Molecular Microbiology 32:789-798.

77. Santos JM, Lobo M, Matos APA, De Pedro MA, Arraiano CM. 2002. The gene bolA regulates dacA (PBP5), dacC (PBP6) and ampC (AmpC), promoting normal morphology in *Escherichia coli*. Molecular Microbiology 45:1729-1740.

78. Attaibi M, den Blaauwen T. 2022. An Updated Model of the Divisome: Regulation of the Septal Peptidoglycan Synthesis Machinery by the Divisome. Int J Mol Sci 23.

79. Abramson J, Adler J, Dunger J, Evans R, Green T, Pritzel A, Ronneberger O, Willmore L, Ballard AJ, Bambrick J, Bodenstein SW, Evans DA, Hung C-C, O'Neill M, Reiman D, Tunyasuvunakool K, Wu Z, Žemgulytė A, Arvaniti E, Beattie C, Bertolli O, Bridgland A, Cherepanov A, Congreve M, Cowen-Rivers AI, Cowie A, Figurnov M, Fuchs FB, Gladman H, Jain R, Khan YA, Low CMR, Perlin K, Potapenko A, Savy P, Singh S, Stecula A, Thillaisundaram A, Tong C, Yakneen S, Zhong ED, Zielinski M, Žídek A, Bapst V, Kohli P, Jaderberg M, Hassabis D, Jumper JM. 2024. Accurate structure prediction of biomolecular interactions with AlphaFold 3. Nature 630:493-500.

80. Käshammer L, van den Ent F, Jeffery M, Jean NL, Hale VL, Löwe J. 2023. Cryo-EM structure of the bacterial divisome core complex and antibiotic target FtsWIQBL. Nat Microbiol 8:1149-1159.

81. Li Y, Gong H, Zhan R, Ouyang S, Park K-T, Lutkenhaus J, Du S. 2021. Genetic analysis of the septal peptidoglycan synthase FtsWI complex supports a conserved activation mechanism for SEDS-bPBP complexes. PLOS Genetics 17:e1009366.

82. Kocaoglu O, Carlson EE. 2015. Profiling of β-lactam selectivity for penicillin-binding proteins in *Escherichia coli* strain DC2. Antimicrob Agents Chemother 59:2785-90.

822 83. Begg KJ, Donachie WD. 1985. Cell shape and division in *Escherichia coli:*
823 experiments with shape and division mutants. J Bacteriol 163:615-22.
824 84. Coltharp C, Buss J, Plumer TM, Xiao J. 2016. Defining the rate-limiting processes of
825 bacterial cytokinesis. Proc Natl Acad Sci U S A 113:E1044-53.
826 85. Schoenemann KM, Krupka M, Rowlett VW, Distelhorst SL, Hu B, Margolin W. 2018.
827 Gain-of-function variants of FtsA form diverse oligomeric structures on lipids and
828 enhance FtsZ protofilament bundling. Mol Microbiol 109:676-693.
829 86. Mueller EA, Westfall CS, Levin PA. 2020. pH-dependent activation of cytokinesis
830 modulates *Escherichia coli* cell size. PLOS Genetics 16:e1008685.
831 87. Dai K, Xu Y, Lutkenhaus J. 1993. Cloning and characterization of *ftsN*, an essential
832 cell division gene in *Escherichia coli* isolated as a multicopy suppressor of
833 *ftsA12*(Ts). J Bacteriol 175:3790-7.
834 88. Gerding MA, Liu B, Bendezu FO, Hale CA, Bernhardt TG, de Boer PA. 2009. Self-
835 enhanced accumulation of FtsN at Division Sites and Roles for Other Proteins with a
836 SPOR domain (DamX, DedD, and RlpA) in *Escherichia coli* cell constriction. J
837 Bacteriol 191:7383-401.
838 89. Geissler B, Elraheb D, Margolin W. 2003. A gain-of-function mutation in *ftsA*
839 bypasses the requirement for the essential cell division gene *zipA* in *Escherichia*
840 *coli*. Proceedings of the National Academy of Sciences 100:4197-4202.
841 90. Hill NS, Kadoya R, Chattoraj DK, Levin PA. 2012. Cell Size and the Initiation of DNA
842 Replication in Bacteria. PLOS Genetics 8:e1002549.
843 91. Buss J, Coltharp C, Shtengel G, Yang X, Hess H, Xiao J. 2015. A multi-layered protein
844 network stabilizes the *Escherichia coli* FtsZ-ring and modulates constriction
845 dynamics. PLoS Genet 11:e1005128.
846 92. Hirota Y, Ryter A, Jacob F. 1968. Thermosensitive mutants of E. coli affected in the
847 processes of DNA synthesis and cellular division. Cold Spring Harb Symp Quant
848 Biol 33:677-93.
849 93. Chen JC, Weiss DS, Ghigo JM, Beckwith J. 1999. Septal localization of FtsQ, an
850 essential cell division protein in Escherichia coli. J Bacteriol 181:521-30.

851 94. Wijsman HJ, Koopman CR. 1976. The relation of the genes envA and ftsA in
852 Escherichia coli. Mol Gen Genet 147:99-102.
853 95. Herricks JR, Nguyen D, Margolin W. 2014. A thermosensitive defect in the ATP
854 binding pocket of FtsA can be suppressed by allosteric changes in the dimer
855 interface. Mol Microbiol 94:713-27.
856 96. Ishino F, Jung HK, Ikeda M, Doi M, Wachi M, Matsuhashi M. 1989. New mutations fts-
857 36, lts-33, and ftsW clustered in the mra region of the Escherichia coli chromosome
858 induce thermosensitive cell growth and division. J Bacteriol 171:5523-30.
859 97. Tsang MJ, Bernhardt TG. 2015. A role for the FtsQLB complex in cytokinetic ring
860 activation revealed by an ftsL allele that accelerates division. Mol Microbiol 95:925-
861 44.
862 98. Begg KJ, Hatfull GF, Donachie WD. 1980. Identification of new genes in a cell
863 envelope-cell division gene cluster of Escherichia coli: cell division gene ftsQ. J
864 Bacteriol 144:435-7.
865 99. Sham L-T, Butler EK, Lebar MD, Kahne D, Bernhardt TG, Ruiz N. 2014. MurJ is the
866 flippase of lipid-linked precursors for peptidoglycan biogenesis. Science 345:220-
867 222.
868 100. Ruiz N. 2008. Bioinformatics identification of MurJ (MviN) as the peptidoglycan lipid
869 II flippase in *Escherichia coli*. Proceedings of the National Academy of Sciences
870 105:15553-15557.
871 101. Marquardt JL, Siegele DA, Kolter R, Walsh CT. 1992. Cloning and sequencing of
872 Escherichia coli murZ and purification of its product, a UDP-N-acetylglucosamine
873 enolpyruvyl transferase. J Bacteriol 174:5748-52.
874 102. Gundavarapu B, Nallamotu KC, Murapaka VV, Venkataraman B, Saisree L, Reddy M.
875 2025. Identification of SanA as a novel regulator of peptidoglycan biogenesis in
876 *Escherichia coli*. PLoS Genet 21:e1011712.
877 103. Li GW, Burkhardt D, Gross C, Weissman JS. 2014. Quantifying absolute protein
878 synthesis rates reveals principles underlying allocation of cellular resources. Cell
879 157:624-35.

880 104. Heijenoort Yv, Gómez M, Derrien M, Ayala J, Heijenoort Jv. 1992. Membrane
881 intermediates in the peptidoglycan metabolism of *Escherichia coli:* possible roles of
882 PBP 1b and PBP 3. Journal of Bacteriology 174:3549-3557.
883 105. Marmont LS, Orta AK, Baileeves BWA, Sychantha D, Fernández-Galliano A, Li YE,
884 Greene NG, Corey RA, Stansfeld PJ, Clemons WM, Jr., Bernhardt TG. 2024. Synthesis
885 of lipid-linked precursors of the bacterial cell wall is governed by a feedback control
886 mechanism in *Pseudomonas aeruginosa*. Nat Microbiol 9:763-775.
887 106. Wissel MC, Weiss DS. 2004. Genetic analysis of the cell division protein FtsI (PBP3):
888 amino acid substitutions that impair septal localization of FtsI and recruitment of
889 FtsN. J Bacteriol 186:490-502.
890 107. Silhavy TJ, Berman ML, Enquist LW. 1984. Experiments with gene fusions. Cold
891 Spring Harbor Laboratory.
892 108. Datsenko KA, Wanner BL. 2000. One-step inactivation of chromosomal genes in
893 *Escherichia coli* K-12 using PCR products. Proceedings of the National Academy of
894 Sciences 97:6640-6645.
895 109. Lutz R, Bujard H. 1997. Independent and tight regulation of transcriptional units in
896 *Escherichia coli* via the LacR/O, the TetR/O and AraC/I1-I2 regulatory elements.
897 Nucleic Acids Res 25:1203-10.
898 110. Hankins JV, Madsen JA, Needham BD, Brodbelt JS, Trent MS. 2013. The outer
899 membrane of Gram-negative bacteria: lipid A isolation and characterization.
900 Methods Mol Biol 966:239-258.
901 111. Deatherage DE, Barrick JE. 2014. Identification of mutations in laboratory-evolved
902 microbes from next-generation sequencing data using breseq. Methods Mol Biol
903 1151:165-88.
904 112. Bolger AM, Lohse M, Usadel B. 2014. Trimmomatic: a flexible trimmer for Illumina
905 sequence data. Bioinformatics 30:2114-20.
906 113. Langmead B, Salzberg SL. 2012. Fast gapped-read alignment with Bowtie 2. Nat
907 Methods 9:357-9.

114. Singer M, Baker TA, Schnitzler G, Deischel SM, Goel M, Dove W, Jaacks KJ, Grossman AD, Erickson JW, Gross CA. 1989. A collection of strains containing genetically linked alternating antibiotic resistance elements for genetic mapping of Escherichia coli. Microbiol Rev 53:1-24.
115. Fu G, Bandaria JN, Le Gall AV, Fan X, Yildiz A, Mignot T, Zusman DR, Nan B. 2018. MotAB-like machinery drives the movement of MreB filaments during bacterial gliding motility. Proceedings of the National Academy of Sciences 115:2484-2489.
116. Zhang H, Venkatesan S, Ng E, Nan B. 2023. Coordinated peptidoglycan synthases and hydrolases stabilize the bacterial cell wall. Nature Communications 14:5357.
117. Allen M, Poggiali D, Whitaker K, Marshall T, van Langen J, Kievit R. 2021. Raincloud plots: a multi-platform tool for robust data visualization [version 2; peer review: 2 approved]. Wellcome Open Research 4.
118. Ducret A, Quardokus EM, Brun YV. 2016. MicrobeJ, a tool for high throughput bacterial cell detection and quantitative analysis. Nat Microbiol 1:16077.

924 **FIGURES AND LEGENDS**

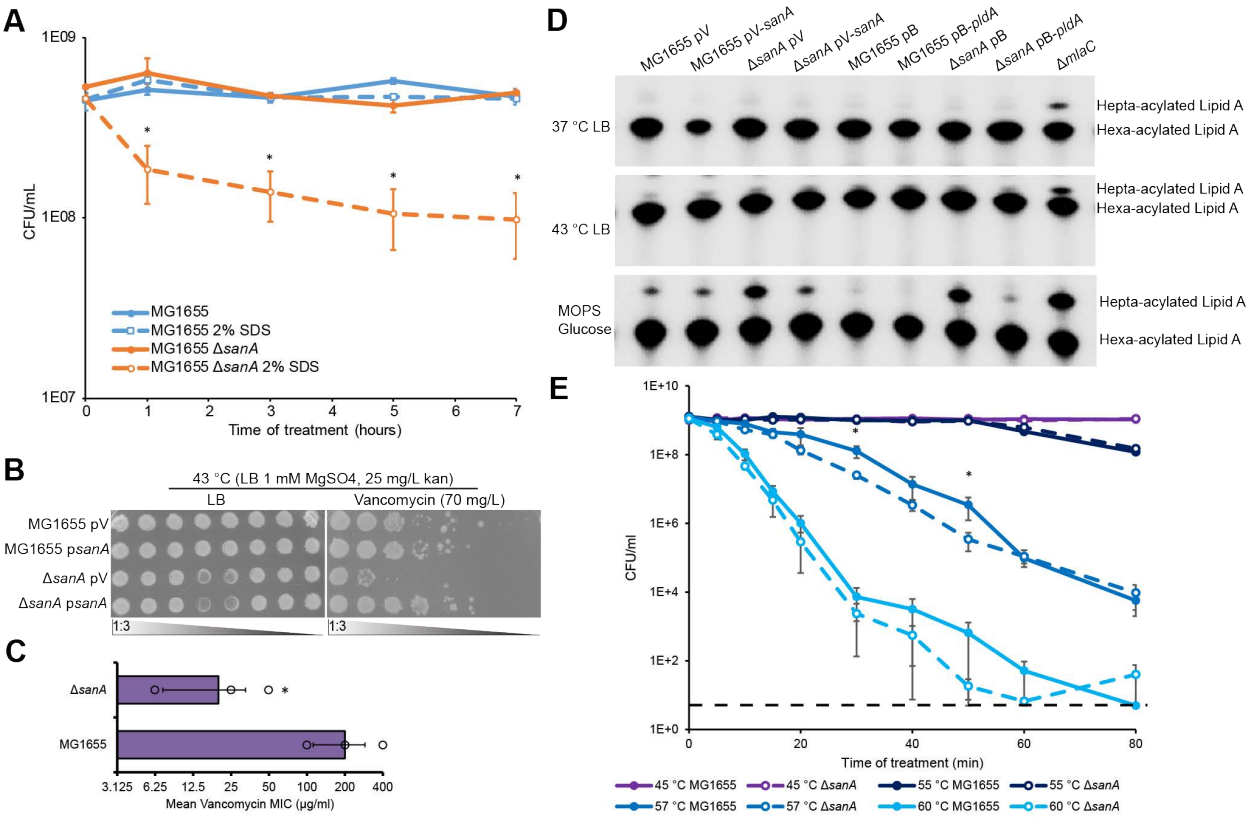

925

926 **Figure 1: Loss of SanA causes increased envelope permeability and low levels of temperature**
927 **sensitivity. (A)** The indicated strains were grown to carbon-limited stationary phase and then treated
928 with SDS EDTA or a vehicle control and viability was assayed by CFU. The Δ*sanA* strain is significantly
929 more sensitive to SDS than the wild-type strain from early time points post treatment. **(B)** The
930 sensitivity of the indicated strains to vancomycin when grown at 43 °C was assayed by EOP. Plates
931 were supplemented with $MgSO_4$ to support growth. The Δ*sanA* strain was more sensitive to
932 vancomycin than the wild-type strain and this sensitivity could be complemented with plasmid
933 based expression of *sanA*. **(C)** To confirm a true change in vancomycin resistance, the MIC for
934 vancomycin was assayed for the wild-type and Δ*sanA* strain. The Δ*sanA* strain was significantly more
935 sensitive to vancomycin than the wild-type strain. **(D)** Modifications to LPS were assayed by thin layer
936 chromatography (TLC) for strains grown in the indicated conditions. The bands for hexa- and hepta-
937 acylated Lipid A are shown. The Δ*sanA* strain shows an increase in hepta-acylated Lipid A which can
938 be mitigated by complementation of *sanA* or overexpression of *pldA*. The *mlaC* strain is known to
939 have an increase in phospholipids in the outer leaflet of the OM (65) and serves as a control. **(E)** Cells
940 were grown to carbon-limited stationary phase at 37 °C and then their ability to survive at the

941 indicated temperatures was assayed. The Δ*sanA* strain shows a significant decrease in survival at 57
942 °C. Quantitative data are the average of three biological replicates ± the SEM. For MICs, data are
943 shown as the geometric average with individual data points. Images are representative of three
944 independent experiments. * p<0.05 by the Mann Whitney Test.

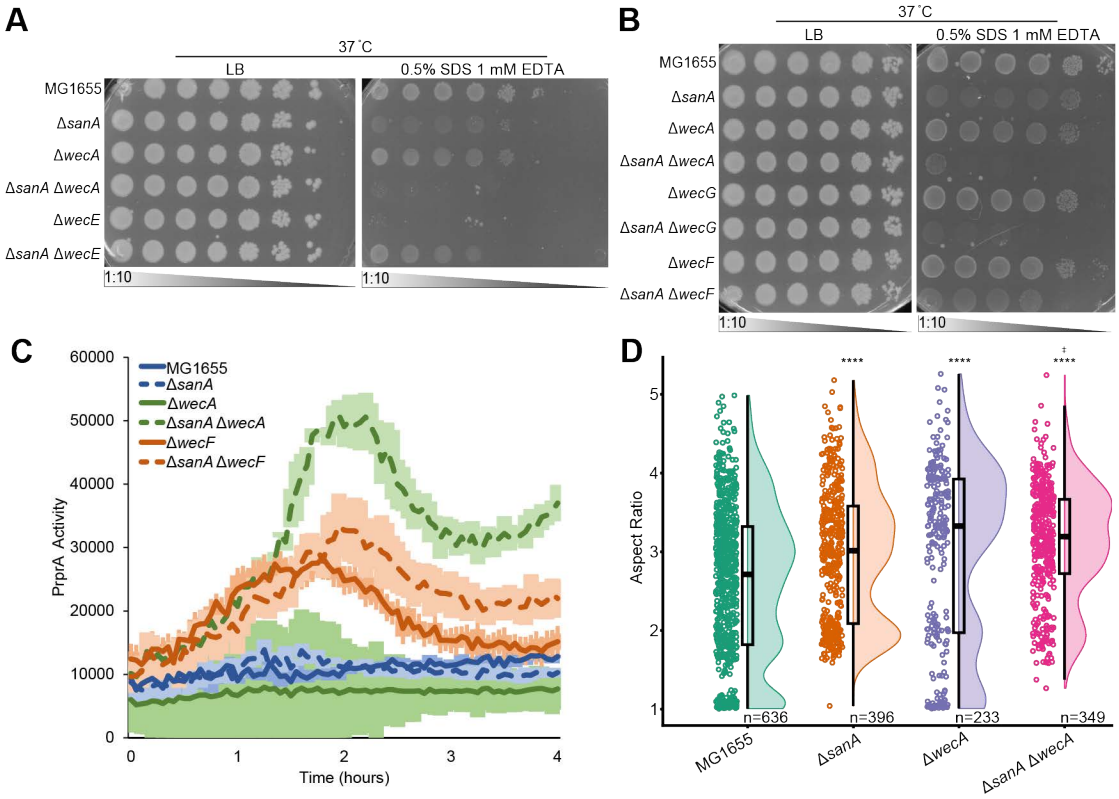

945

946 **Figure 2: SanA shows genetic interactions with ECA synthesis mutations differentially affecting**
947 **PG stress. (A-B)** The indicated strains were assayed for SDS EDTA resistance by EOP. Images are
948 representative of three independent experiments. (A) A double mutant of Δ*sanA* Δ*wecA* showed
949 synthetic SDS EDTA sensitivity, while Δ*sanA* suppressed the SDS EDTA sensitivity of the Δ*wecE* strain.
950 (B) Double mutants of each ECA transglycosylase showed less SDS EDTA sensitivity than the
951 previous strain. **(C)** Activation of the Rcs stress response in the indicated strains was assayed using
952 a *luxCDABE* reporter. Data are shown as luminescence relative to OD_{600}. Data are the average of three
953 biological replicates ± the SEM. **(D)** Cell shape of the indicated strains was assayed, and the aspect
954 ratio (length/width) was calculated. Raincloud plots are shown with individual data points, the
955 population distribution, and a box plot. **** p<0.00005 vs. wild type MG1655 by Wilcoxon Test; ‡
956 p<0.05 vs. the Δ*sanA* Δ*wecA* strain by Wilcoxon Test.

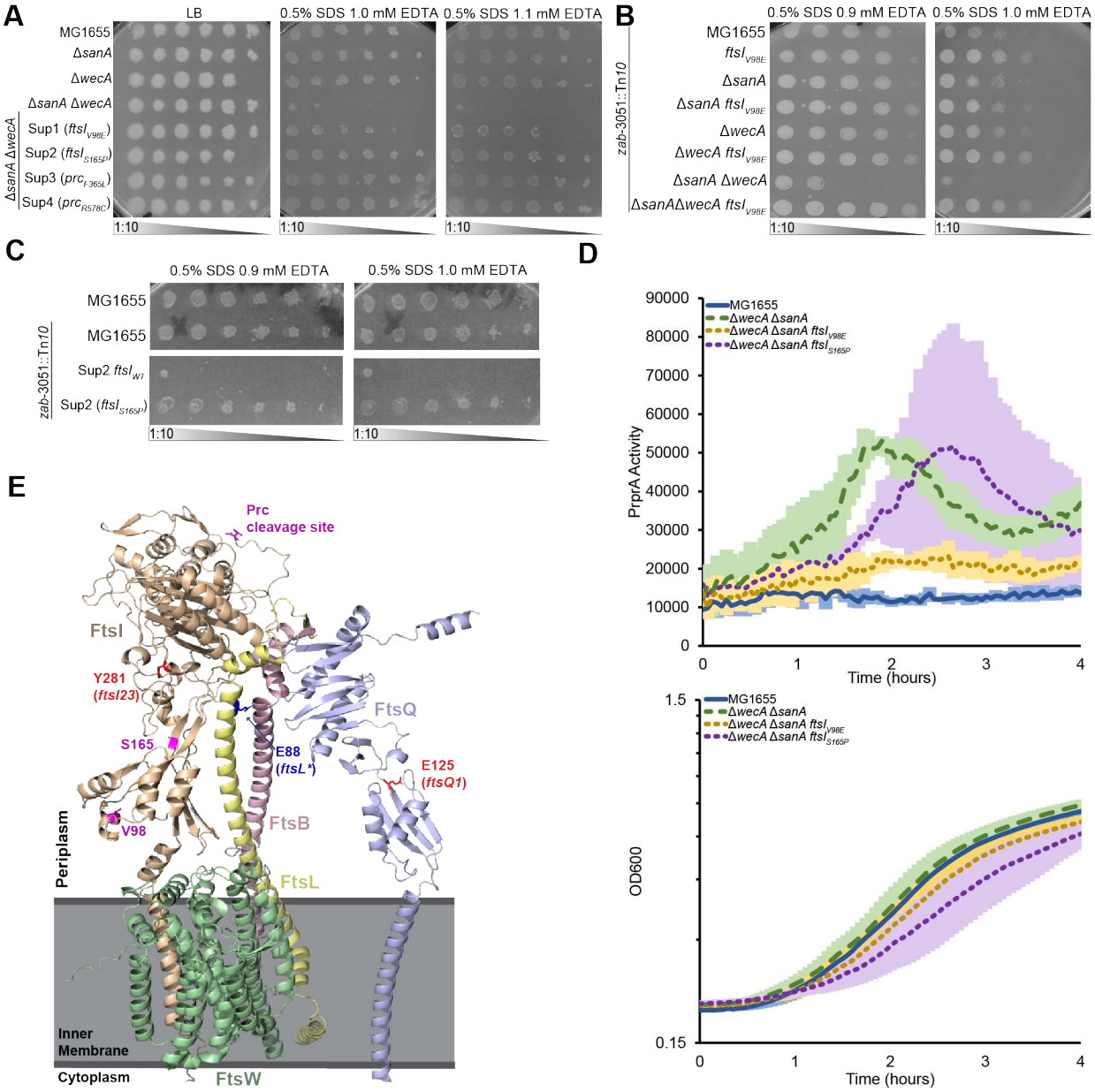

Figure 3: The SDS EDTA of a Δ*sanA* Δ*wecA* strain can be suppressed through mutations to *ftsI* and *prc*. (A-B) The SDS EDTA sensitivity of the indicated strains was assayed by EOP. Images are representative of three independent experiments. (A) Suppressor mutations show increased SDS EDTA resistance compared to the parent Δ*sanA* Δ*wecA* strain. (B) A linked Tn*10* was used to transfer the $ftsI_{V98E}$ mutation the indicated strains. The $ftsI_{V98E}$ mutation was sufficient for suppression. (C) The $ftsI_{S165P}$ mutation was removed from the indicated suppressor and the loss of this mutation prevented suppression demonstrating that it is necessary for suppression. **(D)** Reporter assays for Rcs activation were performed as in Figure 2C. The P_{rprA} activity (luminescence/OD_{600}) as well as the

966 growth of the strains over time are shown. The *ftsI*$_{V98E}$ mutation suppressed the Rcs activation
967 phenotype of the Δ*sanA* Δ*wecA* strain but the *ftsI*$_{S165P}$ mutation did not. The Δ*sanA* Δ*wecA* strain with
968 the *ftsI*$_{S165P}$ mutation also had a noticeable growth defect. Data are the average of three biological
969 replicates ± the SEM.

970

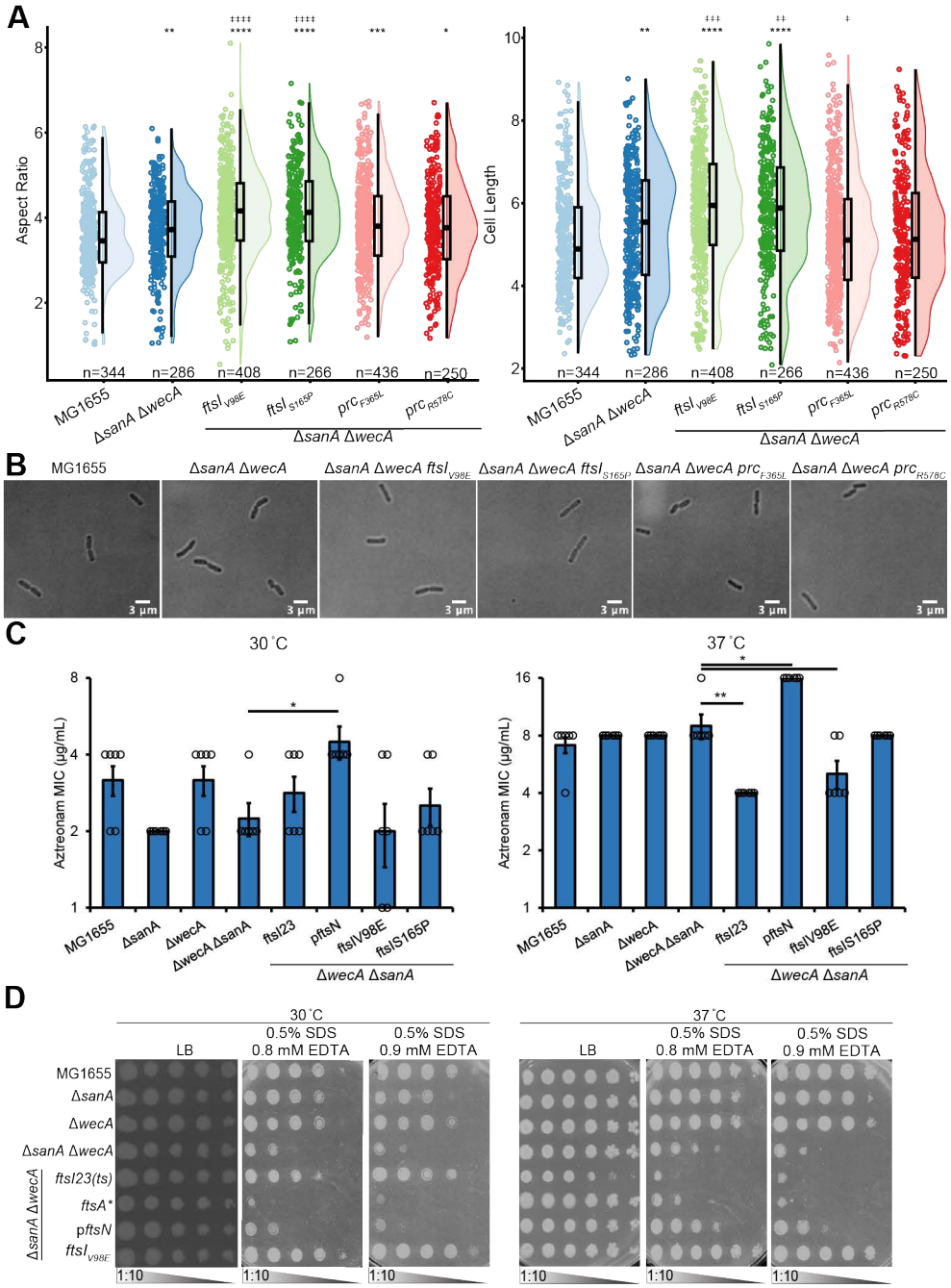

Figure 4: Suppressors of Δ*sanA* Δ*wecA* SDS EDTA sensitivity cause partial loss of FtsI function. **(A)** Cell shape of the indicated strains was assayed, and the aspect ratio (length/width) and cell length are shown. Raincloud plots are shown with individual data points, the population distribution, and a box plot. * p<0.05, **p<0.005, ***p<0.0005, **** p<0.00005 vs. wild type MG1655 by Wilcoxon Test; ‡ p<0.05, ‡‡ p<0.005, ‡‡‡ p<0.0005, ‡‡‡‡ p<0.00005 vs. the Δ*sanA* Δ*wecA* strain by Wilcoxon Test. Mutations in *ftsI* caused the Δ*sanA* Δ*wecA* cells to become significantly longer, while *prc*

978 mutations had less of an effect on length. **(B)** Representative images demonstrating cell shape are
979 shown for the indicated strains. **(C)** The sensitivity of the indicated strains to aztreonam, a β-lactam
980 targeting FtsI, was assayed by MIC. Data are shown as the geometric average of six biological
981 replicates ± the SEM with individual data points. * $p<0.05$, ** $p<0.005$ by Mann-Whitney Test. *ftsI23*
982 and overexpression of *ftsN* serve as controls for decreased and increased activity of FtsI,
983 respectively. The $ftsI_{V98E}$ mutation caused a significant increase in aztreonam sensitivity at 37 °C,
984 indicating decreased FtsI transpeptidase activity. **(D)** The SDS EDTA sensitivity of the indicated
985 strains was assayed by EOP at both 30 and 37 °C. Of the cell division mutants, only *ftsI23* was able
986 to suppress the SDS EDTA sensitivity of the Δ*sanA* Δ*wecA* strain. Images are representative of three
987 independent experiments.

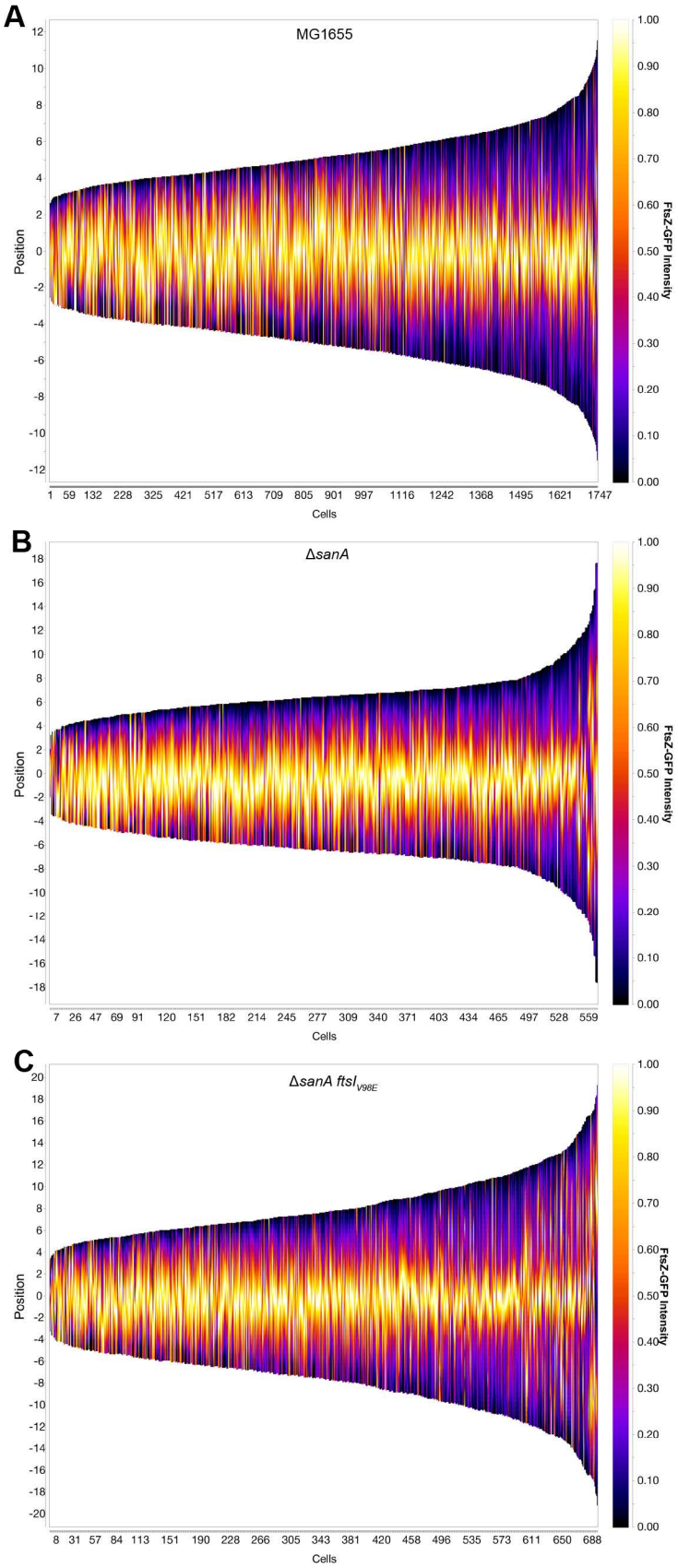
A
MG1655
Position
Cells
FtsZ-GFP Intensity
B
ΔsanA
Position
Cells
FtsZ-GFP Intensity
C
ΔsanA ftsI V98E
Position
Cells
FtsZ-GFP Intensity

988

989 **Figure 5: Loss of SanA does not affect localization of FtsZ.** The FtsZ-GFP localization was assayed
990 in the wild-type strain (A), the Δ*sanA* strain (B), and the Δ*sanA* strain carrying the *ftsI*$_{V98E}$ mutation (C).
991 Demographs were computed using the locational data with cells arranged from shortest to longest.
992 No significant differences in FtsZ localization were observed.

993

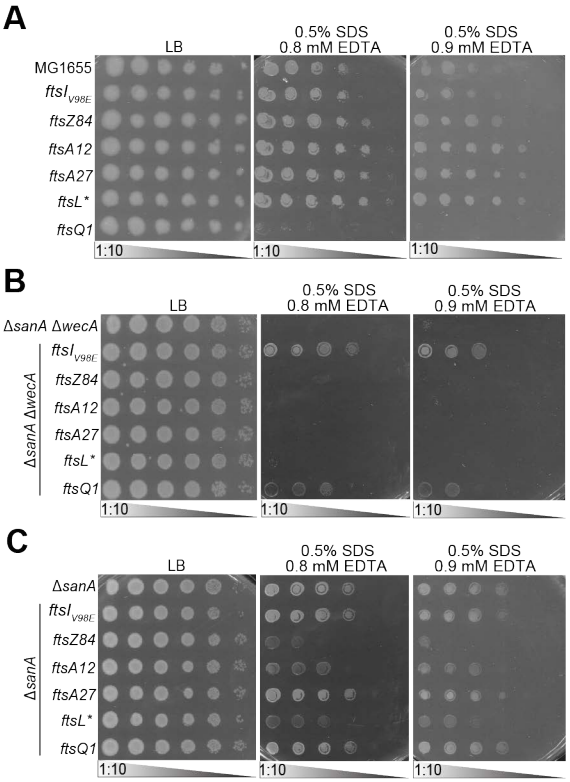

994

995 **Figure 6: Suppression of Δ*sanA* Δ*wecA* phenotypes is linked to septal PG synthesis and not**
996 **divisome assembly.** EOPs were performed at 30 °C to assay the SDS EDTA sensitivity of the indicated
997 strains. The effect of cell division mutations in a wild-type background (A), a Δ*sanA* Δ*wecA*
998 background (B), and a Δ*sanA* background (C) are shown. Images are representative of three
999 independent experiments. **(A)** Only the *ftsQ1* mutation causes SDS EDTA sensitivity in a wild-type
1000 background. **(B)** Of the assayed mutations, only *ftsQ1* suppressed the SDS EDTA sensitivity of the
1001 Δ*sanA* Δ*wecA* strain, while earlier loss-of-function mutations in divisome assembly or gain-of-
1002 function mutations in septal PG synthesis did not. **(C)** The *ftsZ84, ftsA12,* and *ftsL** mutations make
1003 the Δ*sanA* strain more sensitive to SDS EDTA.

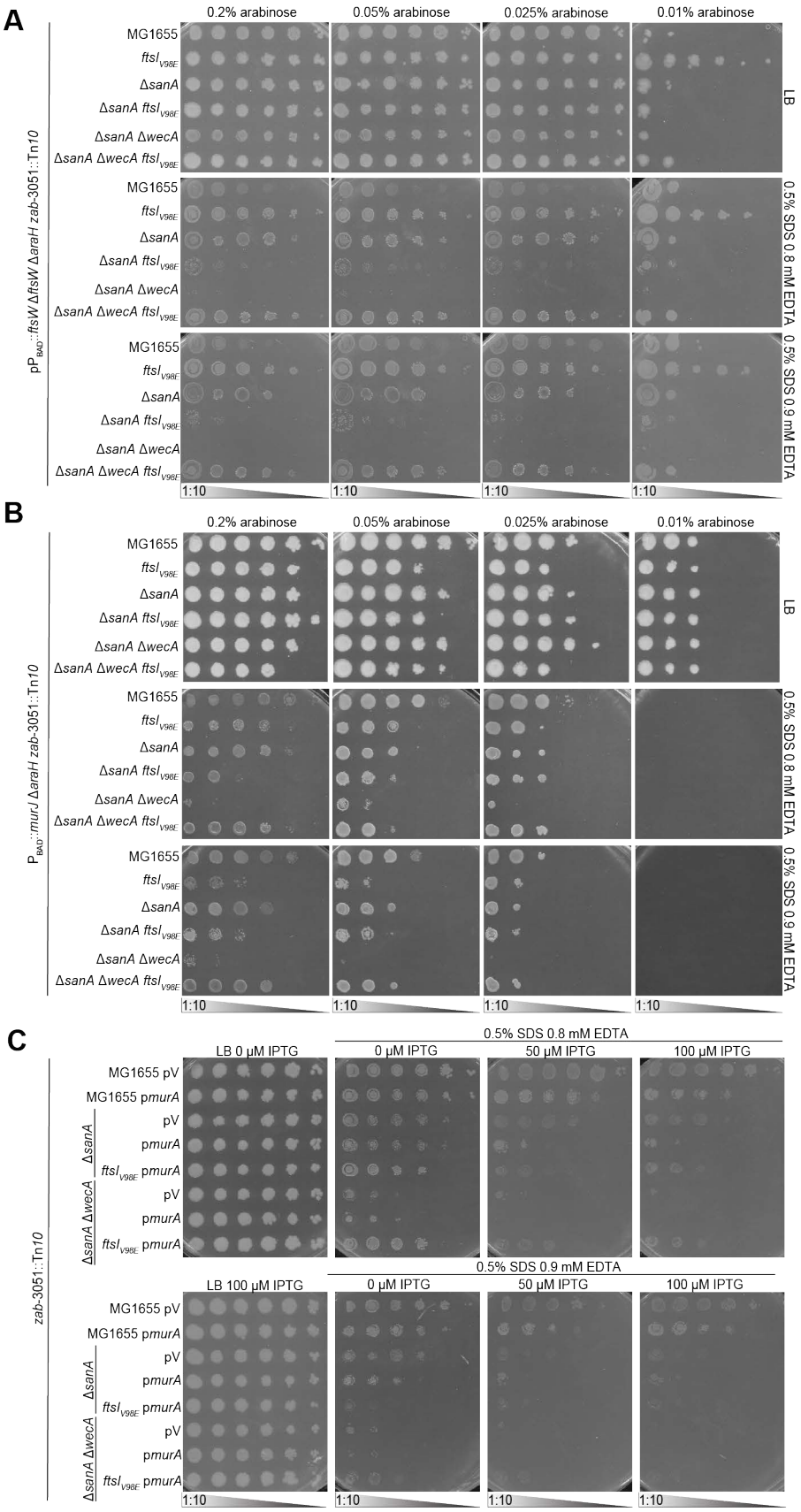
A
0.2% arabinose
0.05% arabinose
0.025% arabinose
0.01% arabinose
MG1655
ftsI V98E
ΔsanA
ΔsanA ftsI V98E
ΔsanA ΔwecA
ΔsanA ΔwecA ftsI V98E
LB
0.5% SDS 0.8 mM EDTA
0.5% SDS 0.9 mM EDTA
pP BAD::ftsW ΔftsW ΔaraH zab-3051::Tn10
1:10
B
P BAD::murJ ΔaraH zab-3051::Tn10
C
LB 0 μM IPTG
0.5% SDS 0.8 mM EDTA
0 μM IPTG
50 μM IPTG
100 μM IPTG
LB 100 μM IPTG
0.5% SDS 0.9 mM EDTA
MG1655 pV
MG1655 pmurA
ΔsanA
ΔsanA ΔwecA
zab-3051::Tn10

1004

1005 **Figure 7: SanA membrane permeability phenotypes are tied to lipid II availability and FtsW**
1006 **activity.** EOPs were performed to assay SDS EDTA resistance in the following strains in the indicated
1007 conditions. Images are representative of three independent experiments. **(A)** FtsW depletion strains
1008 were constructed by deleting *ftsW* in strains carrying a plasmid-based copy of *ftsW* under an
1009 arabinose-inducible promoter. Deletion of *araH*, an inducible arabinose permease, ensures linear
1010 induction. Wild-type cells carrying the $ftsI_{V98E}$ mutation could grow at a lower arabinose
1011 concentration, indicating increased activity of FtsW. Interestingly, this increased activity is not
1012 observed with the $ftsI_{V98E}$ mutation in the Δ*sanA* or Δ*sanA* Δ*wecA* strains. **(B)** MurJ depletion
1013 constructs were made by transduction of an arabinose inducible promoter to replace the native *murJ*
1014 promoter. Depletion of MurJ did not prevent suppression of Δ*sanA* Δ*wecA* SDS EDTA sensitivity by the
1015 $ftsI_{V98E}$ mutation. **(C)** An IPTG inducible *murA* overexpression plasmid or a vector control were
1016 introduced into the indicated strains. Overexpression of *murA* in a Δ*sanA* strain phenocopies the SDS
1017 EDTA sensitivity of the Δ*sanA* Δ*wecA* strain and this sensitivity can be suppressed by the $ftsI_{V98E}$
1018 mutation.